

Advances in SnO₂ for Efficient and Stable n-i-p Perovskite Solar Cells

So Yeon Park and Kai Zhu*

Dr. S. Y. Park, Dr. K. Zhu*

Chemistry and Nanoscience Center, National Renewable Energy Laboratory, Golden, CO 80401, USA.

*E-mail: Kai.Zhu@nrel.gov

Keywords: Perovskite solar cells, electron transport layer, semiconducting oxide layer, SnO₂

Abstract:

Perovskite solar cells (PSCs) based on the regular n-i-p device architecture have reached above 25% certified efficiency with continuously reported improvements in recent years. A key common factor for these recent breakthroughs is the development of SnO₂ as an effective electron transport layer in these devices. In this review, we discuss the key advances in SnO₂ development, including various deposition approaches and surface treatment strategies, to enhance the bulk and interface properties of SnO₂ for highly efficient and stable n-i-p PSCs. We also discuss the general materials chemistry associated with SnO₂ along with the corresponding materials challenges and improvement strategies, focusing on defects, intrinsic properties, and impact on device characteristics. Finally, we highlight some SnO₂ implementations related to scalable processes and flexible devices, and we also provide our perspective on the future development of efficient and stable large-scale perovskite solar modules.

This article has been accepted for publication and undergone full peer review but has not been through the copyediting, typesetting, pagination and proofreading process, which may lead to differences between this version and the [Version of Record](#). Please cite this article as [doi: 10.1002/adma.202110438](https://doi.org/10.1002/adma.202110438).

This article is protected by copyright. All rights reserved.

1. Introduction

Perovskite solar cells (PSCs) are considered a disruptive next-generation solar cell technology due to the extraordinary optoelectronic characteristics of perovskites.^[1-3] During the past decade, rapid and continuous advances in perovskite material and device stack have resulted in unprecedented enhancement in their power conversion efficiency (PCE) from 3.8% to 25.5%, as well as impressive improvements in operational stability, showing high potential for commercial applications.^[2, 4-6]

Among various PSC device architectures, the n-i-p configuration is regarded as the normal device structure, since PSCs were initially developed from dye-sensitized solar cells by using perovskite absorber instead of dye sensitizers.^[3, 7-10] The n-i-p device stack generally consists of a transparent conductive oxide (TCO), dense and/or mesoporous n-type electron transport layer (ETL), perovskite absorber layer, p-type hole transport layer (HTL), back contact electrode, and sometimes additional interfacial layers to achieve better performance. The charge transport layers, including both ETL and HTL, are important for separating and extracting selected photogenerated carriers and blocking counter charge carriers; an effective ETL/HTL can minimize interfacial charge accumulation and recombination.^[9] In an n-i-p-structured PSC, the perovskite layer is coated on the n-type ETL, and the surface area and surface chemistry of the ETL directly affect the deposition and quality of the perovskite layer. Thus, ETL development has become one of the most important scientific subjects for developing highly efficient and stable n-i-p PSCs.

To date, the commonly studied ETLs include n-type semiconducting oxides (e.g., TiO₂, SnO₂, ZnO, Zn₂SnO₄, BaSnO₃) and organics (e.g., phenyl-C₆₁-butyric acid methyl ester [PCBM] and C₆₀).^[7, 10-17] Key properties of ETLs include the proper band energy alignment with perovskite layer, high transmittance with wide bandgap, and high conductivity. Traditionally, the compact TiO₂/mesoporous TiO₂ stack was a key component in efficient n-i-p PSCs, owing to its well-established deposition methods and suitable optoelectronic properties. However, TiO₂ exhibits drawbacks—such as photocatalytic properties under illumination and high-temperature annealing required to achieve proper crystallinity—which can limit PSCs for commercialization.^[18] Many researchers have explored alternative candidates to replace TiO₂, targeting simple and low-temperature fabrication processes with low cost, good reproducibility, and high chemical stability.

Among various candidates, SnO₂ stands out as a promising ETL that has received significant attention in recent years,^[19-22] with the best PCE of SnO₂-based n-i-p PSCs exceeding 25%.^[23] The SnO₂ ETL often exhibits several preferred features such as wide bandgap with high transmittance, good

This article is protected by copyright. All rights reserved.

charge mobility, proper band offsets relative to common perovskites, low-temperature processable synthesis, and decent chemical stability, all of which make SnO₂ ETLs great candidates for highly efficient and stable PSCs.^[24, 25]

In this review, we highlight the main advances in the development of SnO₂ for highly efficient and stable PSCs, with a focus on the n-i-p device configuration. To help understand the research trend of SnO₂-based PSCs, we first provide an overview of key approaches leading to record PCEs based on the development of SnO₂ deposition methods in recent years. Next, we focus on the materials chemistry associated with SnO₂, including defects, intrinsic properties, and impact on device characteristics. We discuss the issues and challenges related to SnO₂ development and SnO₂/perovskite interface optimization, as well as various strategies developed to address these issues in recent years. We also highlight some SnO₂ implementations related to scalable processes and flexible devices that are attractive to industry. Finally, we review the key challenges and provide our perspective on the future development of efficient, stable, printable, and large-scale perovskite solar modules.

2. Overview of SnO₂ Development for Perovskite Solar Cells

As previously mentioned, TiO₂-based n-i-p-structured PSCs have been developed since the beginning of the PSC field and are still actively reported in the literature. The high-temperature (~500°C) sintering of anatase TiO₂ films^[5, 15, 26] and the general photocatalytic properties of TiO₂ have prompted many researchers to search for alternatives. Recent years have seen a surge in interest in utilizing SnO₂ (**Figure 1a, inset**)^[27-31] along with other candidates (e.g., ZnO, Zn₂SnO₄, BaSnO₃, PCBM, and C₆₀) as an ETL for PSC fabrication.^[7, 10-17] Compared to conventional TiO₂, SnO₂ exhibits good optical transmittance and high charge mobility for effective electron extraction. Moreover, SnO₂ is more stable than TiO₂ under ultraviolet (UV) light and is compatible with low-temperature processing.^[32]

During the past several years, there has been substantial progress of SnO₂-based PSCs. These advances are largely driven by progress in the development of SnO₂ ETL deposition methods and interfacial engineering between SnO₂ and perovskite layer. **Figure 1b** summarizes the main achievements in the development of SnO₂-based n-i-p-structured PSCs. The advances of SnO₂ ETL deposition methods and interfacial engineering have improved SnO₂ properties (e.g., defects and band alignment) and enabled large-scale, efficient, and stable devices.^[33-35]

This article is protected by copyright. All rights reserved.

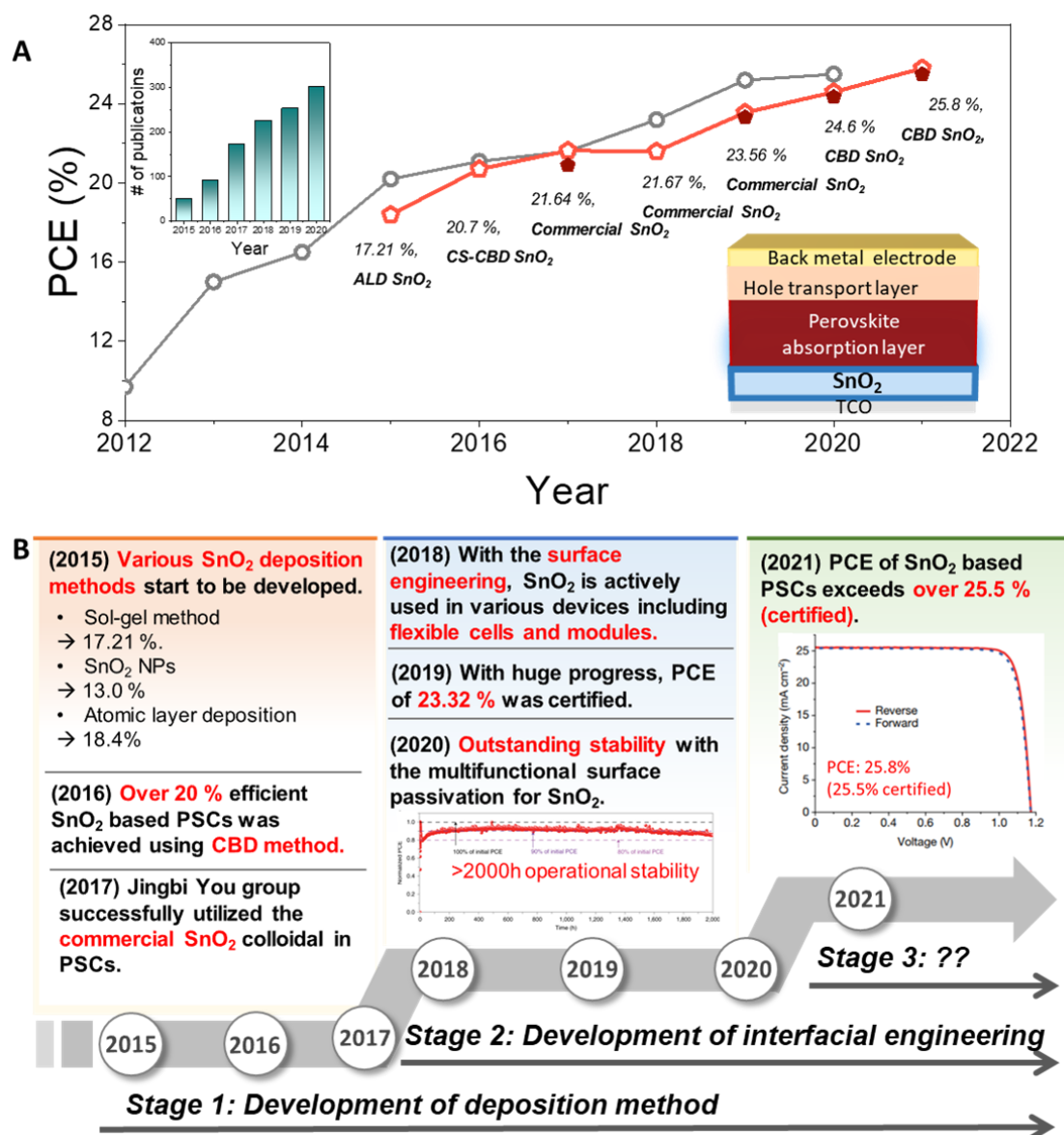


Figure 1. a) Record PCE values for n-i-p PSCs employing SnO₂ as an ETL with comparison to highest-certified PCE in each year (inset: number of published papers per year, calculated from the Scopus database, using the keywords “SnO₂,” “tin oxide,” and “perovskite solar cells”). Open circles: certified PCE for n-i-p PSCs; open pentagons: reported PCE for SnO₂-based PSCs; solid pentagons: certified PCE for SnO₂-based PSCs.^[6, 27, 28, 30, 31, 36-38] b) Historical progress of efficient SnO₂ ETLs, highlighting the important milestones; the key approaches leading to record efficiencies are indicated. Reproduced with permission.^[31, 38] Copyright 2020, 2021, Nature Publishing Group.

Table 1. PCE summary of SnO₂-based PSCs depicted in **Figure 1a**.

This article is protected by copyright. All rights reserved.

Year	SnO ₂ deposition method	SnO ₂ surface treatment	Device structure	PCE (%) (certified PCE)	Ref
2015	ALD (TDMASn)	-	FTO/SnO ₂ /(FAPbI ₃) _{0.85} (MAPbBr ₃) _{0.15} /Spiro- o-OMeTAD/Au	18.4	[30]
2016	SC-CBD SnO ₂	-	FTO/SnO ₂ /Cs/MA/FA perovskite/Spiro- OMeTAD/Au	20.7	[6]
2017	Spin-coating of commercial colloidal SnO ₂	-	ITO/SnO ₂ / (FAPbI ₃) _{0.97} (MAPbBr ₃) _{0.03} (excess Pbl ₂) /Spiro-OMeTAD/Au	21.64 (20.9)	[27]
2018	Spin-coating of commercial colloidal SnO ₂	EDTA	ITO/SnO ₂ /FA _{0.95} Cs _{0.05} Pbl ₃ /Spiro- OMeTAD/Au	21.6	[28]
2019	Spin-coating of commercial colloidal SnO ₂	-	ITO/SnO ₂ /FA _{1-x} MA _x Pbl ₃ /PEAI/Spiro- OMeTAD/Au	23.56 (23.32)	[36]
2020	CBD SnO ₂	-	FTO/SnO ₂ /(FAPbI ₃) _{0.95} (MAPbBr ₃) _{0.05} /BA ₂ Pbl ₄ /Spiro-OMeTAD/Au	24.63 (24.35)	[37]
2021	CBD SnO ₂	Coherent interlayer (FASnCl _x)	FTO/SnO ₂ /FAPbI ₃ /Spiro-OMeTAD/Au	25.8 (25.5)	[31]

In 2015, Ke *et al.* reported low-temperature solution-processed SnO₂ as an ETL for planar PSCs.^[15] The SnO₂ layer was prepared by the sol-gel method based on SnCl₂·2H₂O and 180°C annealing, yielding a device PCE of 17.21%. The 60-nm-thick SnO₂ deposited on fluorine-doped SnO₂ (FTO) showed better transmittance than both the TiO₂ coating and the bare FTO. Since their report, further improvements of solution processing of SnO₂ have been demonstrated by tuning precursor composition, as well as adjusting annealing temperature and environment.^[39, 40] Liu *et al.* used a dual-fuel combustion method to prepare SnO₂ using the precursor solution containing the SnCl₂, NH₄NO₃, and acetylacetonate dissolved in 2-methoxyethanol, and pushed the SnO₂ preparation temperature down to 140°C.^[39] Jung *et al.* adopted tin isopropoxide as a new precursor to prepare the SnO₂ layer with a two-step annealing, which affects the device performance and hysteresis, yielding the best device PCE of 19.4% with 250°C annealing.^[40] Despite early success of sol-gel-processed SnO₂, using this approach alone has so far only reached a PCE of 20.2% with relatively low stability and reliability,^[41, 42] thus, more recent efforts have shifted to alternative approaches.

Solution process using pre-synthesized SnO₂ nanoparticles (NPs) started almost simultaneously with the sol-gel methods in 2015.^[43] Song *et al.* dispersed the SnO₂ NPs (approximately 22–43 nm) in butanol, which was spin-coated on the substrate followed by 200°C annealing for 1 h, yielding a 13%-efficient PSC based on methylammonium lead iodide (MAPbI₃).^[43] The large-sized SnO₂

This article is protected by copyright. All rights reserved.

Accepted Article

NPs would facilitate pinhole formation, causing direct contact between the cathode and perovskite with severe recombination. A big step forward for SnO₂ NP-based PSCs was reported by Jiang *et al.* by using commercial SnO₂ colloidal solution with 3–4-nm-sized SnO₂ NPs.^[36, 44] In these studies, the diluted SnO₂ colloidal solution was spin-coated on the indium-doped SnO₂ (ITO) substrate, followed by 150°C annealing for 30 min in ambient air. The SnO₂ film obtained was dense and pinhole-free with a good transparency, pushing the PCE to a record level of 23.56% with a certified value of 23.32%.^[36] Following these breakthrough studies, the method based on commercial SnO₂ colloidal solution has been widely used in the development of n-i-p PSCs. In addition, various interfacial modification strategies (with details discussed in Section 5) have shown promise for improving the efficiency and stability of SnO₂-based n-i-p PSCs. A recent example demonstrated the use of biguanide hydrochloride (BGCl) as a multifunctional interface modifier to improve the SnO₂/perovskite interface with better energetic alignment and reduced interfacial defects. As a result, the colloidal-SnO₂-based PSCs with BGCl interlayer achieved a PCE of 24.4% with much improved V_{oc} and FF as compared to the control device (22.4%).^[45]

In 2016, Anaraki *et al.* reported another simple, low-temperature, scalable method to prepare SnO₂ ETL based on chemical bath deposition (CBD).^[6] A combination of spin-coating and CBD post-treatment (SC-CBD) of SnO₂ ETL yielded PCEs close to 21%, gaining in device fill factor (FF) when compared to the conformal SnO₂ coating by atomic layer deposition (ALD).^[6, 46] Yoo *et al.* further improved the CBD-based SnO₂ by controlling the complex chemical reactions during SnO₂ deposition, with the corresponding device reaching a certified PCE record of 25.2% from a quasi-steady-state measurement, with 25.3% and 25.4% from for the reverse and forward current density–voltage (J - V) scans, respectively.^[23] Recently, Min *et al.* introduced a strategy to form a coherent interlayer between Cl-bonded CBD SnO₂ and perovskite layers, leading to a demonstration of PSCs with PCE of 25.8% (25.5% certified), which is among the best published SnO₂-based PSCs.^[31]

In addition to solution processing, vapor-based deposition methods (e.g., ALD, pulsed laser deposition [PLD], and sputtering) have also been used to prepare SnO₂ ETL since 2015.^[30, 46, 47] Among these methods, the ALD approach is the most promising due to the uniform and compact coating over large areas and rough substrates. In addition, ALD is flexible with metal precursor and oxygen source (e.g., oxygen plasma, ozone, and H₂O) to make high-quality films with different Sn/O ratios under low process temperatures. Correa-Baena *et al.* reported a low-temperature (118°C) ALD process using tetrakis(dimethylamino) tin(IV) (TDMASn) (tin precursor) and ozone (oxygen source) and showed the PCE >18% with an open-circuit voltage (V_{oc}) >1.19 V.^[30] The device PCE was further improved to >20% with a V_{oc} reaching 1.23 V in 2017.^[47] However, ALD SnO₂ has so far produced PSCs with lower PCEs

This article is protected by copyright. All rights reserved.

than solution-processed SnO₂ and also has a limitation in providing the proper crystallized SnO₂ without post-annealing.

Considering the overall development of SnO₂-based n-i-p PSCs so far, the early-stage research focused on the development of different SnO₂ deposition methods. In the subsequent development stage, various interfacial engineering approaches were reported to improve the SnO₂/perovskite interface, which has enabled significant performance enhancement and easy transition to scalable processes and flexible devices. We summarize the important milestones in the evolution of efficient SnO₂-based n-i-p PSCs in **Figure 1b**. We focus on the fundamental understanding of the basic properties of the SnO₂ ETL and SnO₂-based n-i-p PSCs from the current literature results in Sections 3–7, and we further discuss the challenges and strategies for future advances in SnO₂-based n-i-p PSCs in Section 8.

3. Fundamental Properties and Synthesis of SnO₂

In this section, we review the basic optoelectronic and physicochemical properties of SnO₂. Based on the fundamental properties of SnO₂, we discuss the details of why SnO₂ is a suitable ETL material in PSCs, and what to consider for making a better SnO₂ ETL.

3.1. Electronic Structure and Defect Properties of SnO₂

SnO₂ has several phases such as the rutile-type ($P4_2/mnm$), CaCl₂-type ($Pnmm$), α -PbO₂-type ($Pbcn$), ZrO₂-type orthorhombic phase I ($Pbca$), cotunnite-type orthorhombic phase II ($Pnam$), and fluorite-type ($Fm3m$).^[48, 49] Among these different phases, the rutile-type tetragonal SnO₂ is the most chemically and thermally stable crystalline structure of SnO₂ at ambient pressure, and thus it is the most studied SnO₂ as an n-type semiconducting oxide.^[48, 50]

It is well known that undoped SnO₂ is an n-type semiconductor because of dominant defects of Sn_i and V_o in SnO₂; this also accounts for the nonstoichiometry of this material in the absence of any specific treatments.^[48] As summarized in **Figure 2a**, these defects produce shallow donor levels, accounting for the n-type conduction in undoped SnO₂. Rutile SnO₂ crystals can have various intrinsic point defects (e.g., oxygen and tin vacancies, interstitials, and antisite defects) and extrinsic dopants, mainly affecting the electrical and optical properties and energy level.^[51]

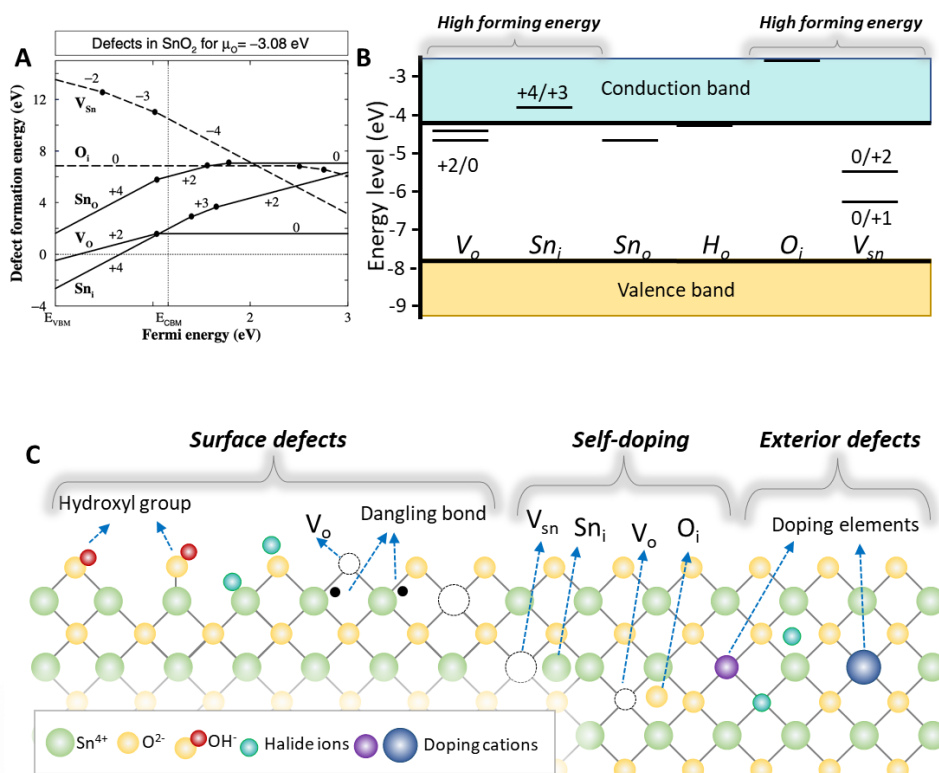


Figure 2. a) Formation energy of intrinsic point defects and H impurity in SnO₂. Reproduced with permission.^[51] Copyright 2002, American Physical Society. b) Schematic representation of defect transition levels in SnO₂. c) Schematic illumination of various possible defects in SnO₂ surface and crystals.

Figure 2b shows the formation energies of various point defects in SnO₂. Sn_i and V_o defects can be formed spontaneously, leading to n-type nonstoichiometric SnO₂.^[50, 51] The Sn_i donor level is fully ionized in the conduction band (CB), whereas the singly-ionized (shallow) and doubly-ionized (deep) oxygen vacancy donor levels are present 0.03 eV and 0.15 eV below the CB minimum, respectively. Thus, oxygen vacancies can strongly affect the electron concentration associated with these two donor levels. The electrical conductivity varies inversely with the oxygen partial pressure, correlating to the number of oxygen vacancies. Note that a reduction in the carrier concentration can be related to a decrease of the densities of V_o and Sn_i defects, or caused by the formation of O_i or V_{Sn} sites, which can offset the n-type defects. Under an oxygen-rich atmosphere, a greater amount of oxygen can be incorporated in the lattice; in this situation, the O_i or V_{Sn} defects with low formation energies are easy to form, whereas the high formation energy of V_o and Sn_i limit their formation, and consequently, the corresponding SnO₂ film can approach its stoichiometry. However, under normal

This article is protected by copyright. All rights reserved.

processing conditions (e.g., ambient air), it is difficult to form O_i and V_{Sn} owing to their high formation energies.^[50, 51]

Doping is commonly used to control the conductivity of SnO_2 .^[52] In general, the ionic radius of the dopant needs to be comparable or smaller than the host ion (Sn^{4+}) to achieve efficient doping. Elements such as Al/In/Ga with lower valence than Sn^{4+} are normally added for p-type doping. These elements can substitute the Sn sites and produce shallow acceptors, leading to increased hole concentration that can effectively reduce the intrinsic n-type conductivity. Other elements such as Li and Mg are also used to tune the doping properties, either as acceptors with O-site substitution, or as donors Sn-site substitution.

Generation of surface defects on SnO_2 can also affect the electrical and chemical characteristics of SnO_2 . Most metal oxides are usually hydroxylated under ambient conditions because univalent anion (like hydroxide ions) can fit closer to the center of a positive charge than the bivalent ions (oxide ions) at the surface.^[53] There are two kinds of hydroxyl groups on the SnO_2 surface: (1) basic terminal hydroxyls binding to one Sn site; and (2) acid bridge hydroxyls binding to two metal sites. In addition, hydroxyl groups and O ions at the surface react with H_2 , and then unsaturated Sn dangling bonds can be generated at the surface by forming H_2O gas.^[54] Thus, numerous Sn dangling bonds on the SnO_2 surface can easily form during the synthesis and fabrication of SnO_2 , and these Sn dangling bonds can absorb O_2 and H_2O in the ambient atmosphere, trap electrons, and form potential barriers to obstruct electrons transport.

We summarize the possible defects in **Figure 2c**, including surface defects, interior defects (self-doping) and exterior defects. By taking advantage of defect management in SnO_2 , various deposition approaches, including both physical and chemical methods, have been used to prepare SnO_2 with suitable optoelectronic properties for a variety of applications (e.g., optoelectronic devices and catalysis). At the same time, it is still challenging to control different kinds of high-density bulk and surface defects to tailor SnO_2 to maximize its function for specific applications.

3.2. Basic Characteristics of SnO_2 as an Electron Transport Layer

The ETL is a crucial part of optoelectronic devices. ETLs for efficient and stable PSCs should satisfy the following requirements: wide-bandgap material with high transparency to minimize parasitic optical loss, proper band alignment with the perovskite absorber layer for efficient charge separation, compact and pinhole-free layer to enable optimum contact and avoid shunting, and high conductivity for electron transport and effective hole-blocking ability. In terms of operational stability, the ETL should also be stable under device operating conditions (e.g., light, heat, and bias voltage) and

This article is protected by copyright. All rights reserved.

no charge accumulation at the perovskite/ETL interface. For an n-i-p device, the optical property of the ETL is particularly important, as the light will pass through the ETL before reaching the perovskite absorber layer. Thus, many device parameters (e.g., short-circuit current density [J_{sc}], V_{oc} , hysteresis, and stability) can be affected by the properties of the ETL and perovskite/ETL interface.

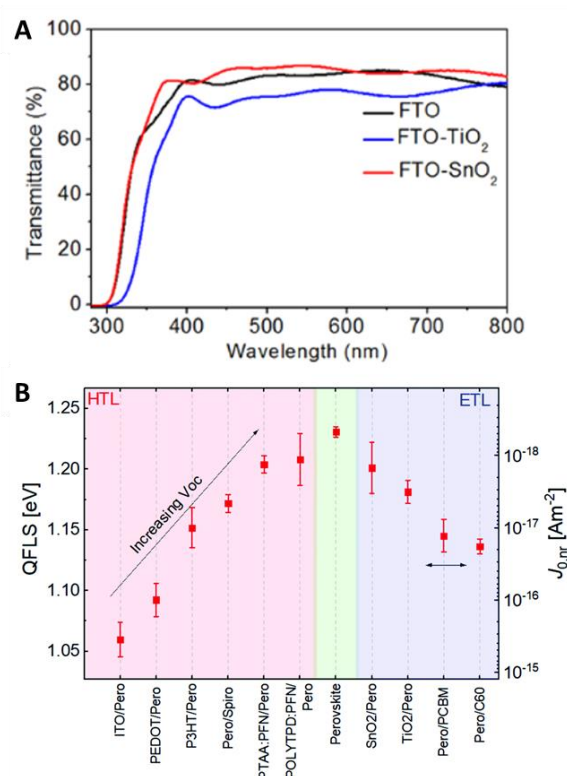


Figure 3. a) Transmission spectra of FTO substrates without and with coating of either a TiO₂ film or SnO₂ nanocrystalline film with a fixed film thickness. Reproduced with permission.^[26] Copyright 2015, Royal Society of Chemistry. b) The quasi-Fermi level splitting (QFLS) of heterojunctions with different hole and electron transporting materials and of the neat absorber layer. Reproduced with permission.^[55] Copyright 2019, Royal Society of Chemistry.

The J_{sc} values of PSCs are obviously the most related to the light-absorption (i.e., perovskite) layer. In n-i-p PSCs, the ETL and TCO layers over the substrate (soda-lime glass or plastic flexible substrate) are also important. Compared to other n-type semiconducting materials, SnO₂ has a remarkably large bandgap (~3.6 to 4.5 eV) and high transparency in the range of 300–1,000 nm).^[6, 24, 25, 56] It is noteworthy that a 60-nm-thick sol-gel-processed SnO₂ film showed better transmittance than both a TiO₂ film with the same thickness and a bare FTO substrate (**Figure 3a**). Furthermore, even though the prepared SnO₂ films for PSCs generally contain many defects because of low processing

This article is protected by copyright. All rights reserved.

temperature, those intrinsic defects (e.g., Sn_i and V_o) only have minor effects on the transparency of SnO_2 in the visible range, owing to a large gap between Fermi level and the CB minimum of SnO_2 .^[52, 57-59]

To obtain a high V_{oc} for efficient PSCs, it is critical to minimize energy losses by reducing carrier trap sites and nonradiative recombination pathways across the entire device stack, including bulk materials and various interfaces.^[55, 60, 61] The maximum achievable V_{oc} of a device stack can be inferred from the quasi-Fermi level splitting (QFLS), which can be determined from the absolute photoluminescence measurement. Stolterfoht *et al.* reported the relationship between V_{oc} and QFLS based on the absolute photoluminescence measurements in PSCs with various charge transport materials.^[55] A comparison of the QFLS obtained on charge transport material/perovskite bilayers shows that the SnO_2 /perovskite interface gives higher QFLS (>1.20 eV) than other ETL materials, with a minimum loss relative to the neat perovskite (1.23 eV), as shown in **Figure 3b**. This implies that additional energy losses and nonradiative recombination at the SnO_2 /perovskite interface would be minor, and the V_{oc} of the corresponding device would be higher compared to other ETL-based devices. However, the mismatch between QFLS and V_{oc} can appear in real devices because of the presence of energy offset and interfacial defects across the device interface. Thus, interfacial engineering for tuning the band offset and surface defect passivation is required to reach the full potential for SnO_2 -based PSCs.

Furthermore, negligible hysteresis index in PSC J - V curves is also an important parameter for consideration when developing devices with enhanced stability.^[62, 63] In general, hysteresis is caused by unbalanced charge extractions and charge recombination/accumulation at the ETL (or HTL)/perovskite interfaces. It has been reported that SnO_2 with high electron mobility and conductivity compared to other oxide semiconductors has advantages for reducing the J - V hysteresis.^[26, 30] However, the defects and improper energy barrier at the SnO_2 /perovskite interface in n-i-p devices can cause a serious J - V hysteresis, and interfacial passivation strategies can mitigate the inherent hysteresis issue related to the SnO_2 layer.^[13, 64]

3.3. General Preparation of SnO_2 Thin Films

SnO_2 ETLs are primarily used for the planar n-i-p PSCs. Thus, various deposition methods have been developed to form conformal, compact, and pinhole-free SnO_2 thin films with optimum conductivity and transparency. Typical methods include solution-process approaches (e.g., sol-gel, combustion methods, CBD, and spin-coating of SnO_2 NP ink) and vapor-process approaches (e.g., sputtering, PLD, and ALD methods).^[65-67]

This article is protected by copyright. All rights reserved.

During the early stage, most widely developed methods are based on spin-coating of sol-gel-based tin precursors or lab-made SnO₂ NPs. The film quality and characteristics of sol-gel-processed SnO₂ films using tin precursors such as SnCl₂·2H₂O and SnCl₄·5H₂O strongly depend on the tin source, solvent, and post-annealing temperature. Most sol-gel-processed SnO₂ layers are prepared by spin-coating the tin chloride (SnCl₂·H₂O) in polar solutions (e.g., water and alcohol), followed by annealing at about 150°C–180°C. Even though the crystallinity of SnO₂ can be improved with annealing at >400°C with increased free electron density, PSCs based on such sol-gel-processed SnO₂ often show worse performance, as high-temperature annealing can cause poor interfacial contact and poor film compactivity.^[68] To circumvent this challenge, other post-annealing methods have been developed to enable better metal-oxide-metal network formation of SnO₂ at low temperatures, such as UV-assisted and plasma-assisted methods.^[69, 70] Nevertheless, sol-gel processed SnO₂ with low temperature annealing often shows excessive uncertain defects in the bulk as well as on the surface in comparison to other solution deposition methods (e.g., CBD or coating with pre-synthesized colloidal solution). Although interfacial modifications have shown advances for sol-gel SnO₂, the PSC development based on this approach still lags behind other solution approaches in recent years.

For the SnO₂ NP approach, various preparation methods have been developed with different applications.^[24, 67] For application in planar-structured PSCs, the SnO₂ NPs should be well dispersed in proper solvents with minimum residual organic impurities to fabricate a thin and uniform layer with a low post-annealing temperature. Thus, in contrast to those synthesis methods with additional ligands/additives and further washing steps, the sol-gel-based SnO₂ NP synthesis methods under low temperature (<80°C) or at room temperature are preferred for direct fabrication of SnO₂ film without additional steps. With this direct fabrication process, hydrolysis of Sn²⁺ ions and oxidation could take place to form SnO₂ during refluxing the prepared solution at ambient conditions.^[67] In another study, Jiang *et al.* reported the use of a commercial SnO₂ colloidal solution to successfully form a compact and uniform SnO₂ film by spin-coating the diluted colloidal solution followed by 150°C annealing.^[44] Since crystallinity and bulk defects can be controlled in those pre-synthesized SnO₂ colloids or NPs before coating, this method is simple and reproducible with easy control of the film thickness by adjusting solution concentration. Many research groups have adopted this method and made further improvements using various additive and passivation strategies. Note that the colloidal SnO₂ NP inks can also be used for slot-die, blade, and spray coating for scaling up development.^[35, 71, 72]

Chemical bath deposition method is one of the representative solution methods for directly fabricating SnO₂ thin films on the substrate. CBD-based SnO₂ deposition on a substrate is managed by controlling the nucleation on substrate and the subsequent growth of SnO₂. In typical CBD SnO₂

This article is protected by copyright. All rights reserved.

growth, the hydrophilic substrates are vertically dipped in the acidic SnCl_2 solution for reaction/deposition; an oven is normally used to control the deposition temperature. The SnCl_2 solution for CBD growth is normally prepared using deionized water with additional urea as a binder and acid (e.g., mercaptoic or hydrochloric acid) as a stabilizer.^[23, 37, 73] The key to form a high-quality SnO_2 CBD film relies on controlling the nucleation to form a compact dense film and the intermediate species, which affect defect states of the final SnO_2 film depending on the decomposition pathway of the Sn^{2+} precursor.^[23] In their study, Yoo *et al.* achieved a certified PCE of 25.2% using the CBD SnO_2 .^[23] The CBD method also works for large-area SnO_2 deposition with small modifications.^[35] Despite the advantages associated with the CBD method, frequent bath replacement and large volume of waste solution are critical challenges for commercialization.

For ALD SnO_2 processing, the self-limiting reaction process can provide highly uniform and dense thin films with low processing temperature and high reproducibility, regardless of the roughness and complexity of substrates. However, the ALD process also requires high-level precise control in selecting the tin precursor, reactant, purge sequence, and reaction environment even after ALD deposition, such as the post-annealing step, to make further crystallization and regulate the unreacted precursor (e.g., TDMASn).^[65, 66, 74] Also, similar to the sol-gel process, unclear and incomplete metal-oxide metal network formation in the bulk SnO_2 film is a critical challenge that hinders the achievement of high-performance PSCs based on ALD SnO_2 . Other vapor-based methods for SnO_2 thin film include electron-beam or thermal evaporation, magnetron sputtering, and PLD,^[75-78] which are usually targeted for high reproducibility and large-area deposition towards commercialization. However, these methods are not frequently used because of the demonstrated device performance below expectation.

Despite continued advances in SnO_2 deposition methods, the bare SnO_2 films still present restrictions with the substrate choice, insufficient SnO_2 quality, and large-area application. Many researchers have developed various strategies with additional treatment methods to address these limitations, including bulk crystal modification and interface engineering, which are discussed in detail in Section 5.

4. SnO_2 /Perovskite Interface

When looking back on the recent evolution of SnO_2 -based PSCs with rapid advances at addressing key issues, it is evident that engineering the SnO_2 /perovskite interface represents an active and promising research area for making efficient and stable PSCs. The surface chemistry of SnO_2 can

This article is protected by copyright. All rights reserved.

change during and/or after deposition on the substrate, and it is often quite complicated with different oxidation states (Sn^{2+} and Sn^{4+}), oxygen vacancies, hydroxyl groups, and secondary phases (e.g., SnO , Sn_2O_3 , and $\text{Sn}(\text{OH})_2$).^[23, 79] The exact species and their relative amounts on the SnO_2 films are different depending on the deposition method and annealing condition. These defects and different valences of Sn and O species can modify the energy levels and optical and electrical properties, resulting in changes in charge dynamics and the stability of the SnO_2 /perovskite interface.^[80] In addition, the surface state of SnO_2 can affect the reaction between SnO_2 and perovskite precursor related to the mechanical integrity of SnO_2 /perovskite interfaces and perovskite crystal growth.^[81-83] In this section, we discuss several key aspects of the SnO_2 /perovskite interface, with a focus on the n-i-p device configuration.

4.1. Interfacial Energetics

High electron mobility of SnO_2 can facilitate electron transfer/extraction and reduce charge accumulation/recombination in a device. In addition, the interfacial energy alignment also plays a key role in determining charge dynamics.^[15, 84]

For efficient charge collection from perovskite to ETL, a low CB offset at the ETL/perovskite interface is often required.^[85] A large valence band (VB) offset at the SnO_2 /perovskite interface, along with minimized mid-gap states in SnO_2 , are necessary for effectively blocking hole transport and reducing interfacial recombination. From the work function perspective, a low work function level of ETL compared to the perovskites enables an interfacial band offset for facilitating electron collection (**Figure 4a**).

For a given perovskite composition, the energy alignment at the SnO_2 /perovskite interface directly depends on the CB level of SnO_2 . If the CB level of SnO_2 is lower than that of the perovskite, the energy cliff CB offset (-) is formed with no potential barrier for electrons at the SnO_2 /perovskite interface, which could facilitate recombination from back electron transfer to the interface region. On the other hand, if the CB level of SnO_2 is higher than that of the perovskite, the energy spike CB offset (+) is formed at the SnO_2 /perovskite interface, acting as a barrier to suppress back electron transfer and reduce interfacial recombination.^[86-88] A recent device simulation study showed that for a planar structure FTO/ SnO_2 /MAPbI₃/2,2',7,7'-Tetrakis[N,N-di(4-methoxyphenyl)amino]-9,9'-spirobifluorene (spiro-OMeTAD)/Ag, the interfacial recombination was significantly increased when the CB of SnO_2 was lower than that of perovskite (**Figure 4b**).^[86, 88] Although the spike CB offset can suppress interfacial recombination, it can also inhibit the transport/separation of photogenerated carriers if the

This article is protected by copyright. All rights reserved.

spike CB offset is too high (>0.4 eV). Thus, an optimized SnO_2 /perovskite interface with suitable CB/VB offsets is essential for pushing up the device performance.

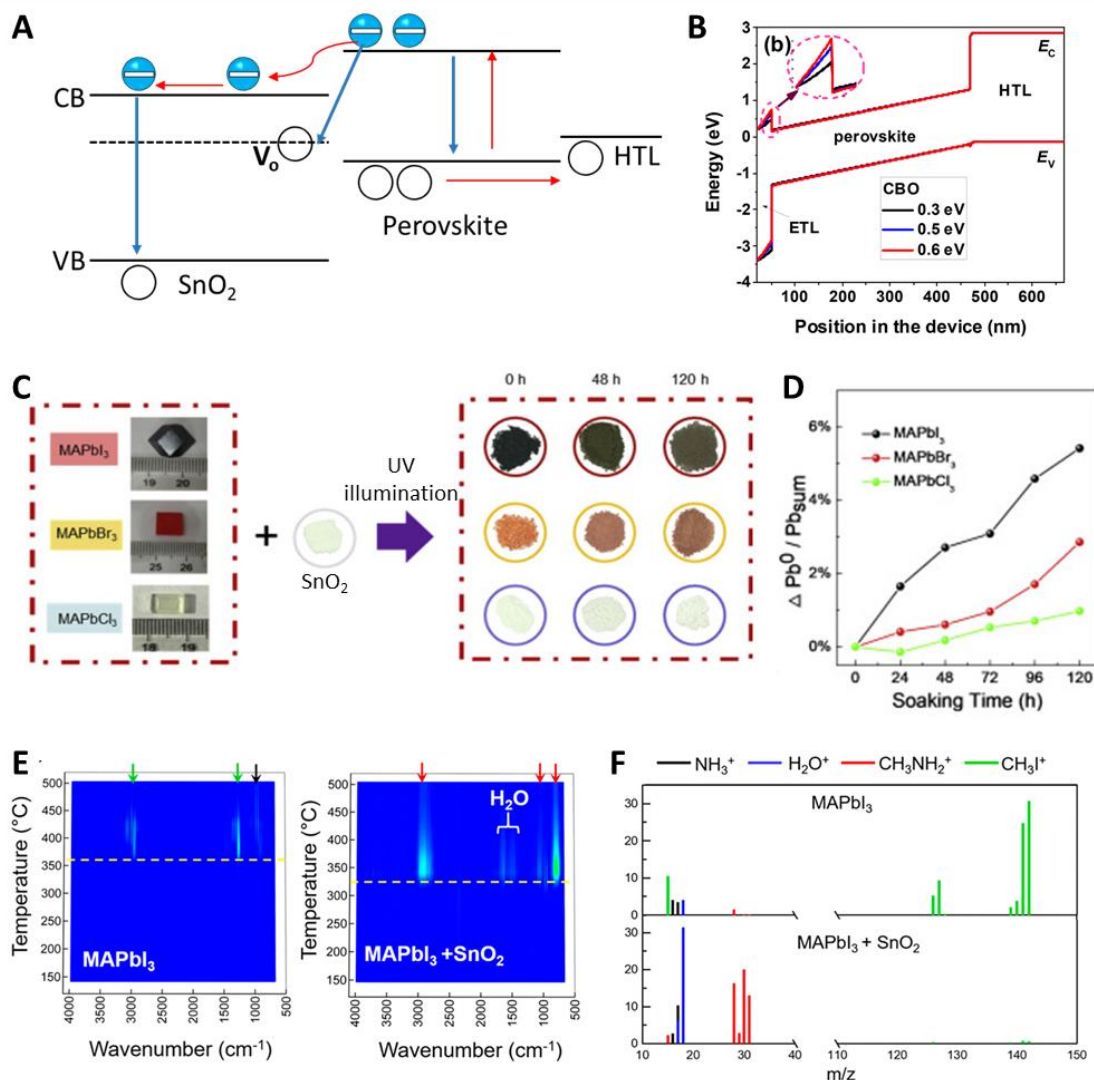


Figure 4. a) General design of energy levels at the SnO_2 /perovskite interface. b) Energy band diagrams for n-i-p PSCs with different positive values of CB offsets. Reproduced with permission.^[86] Copyright 2019, American Chemical Society. c) Photographs of the synthetic perovskite single crystals (MAPbI_3 , MAPbBr_3 , and MAPbCl_3) and the mixtures of single-crystal powder and SnO_2 NP under different UV illumination time. d) $\text{Pb}^0/\text{Pb}_{\text{sum}}$ of MAPbI_3 , MAPbBr_3 , and MAPbCl_3 -based mixtures from the fitted results of X-ray photoelectron spectra. Reproduced with permission.^[89] Copyright 2019, Elsevier. e) 2D contour plots of Fourier-transform infrared spectroscopy (FT-IR) results, and f) mass spectrometry signals with NH_3 , H_2O , CH_3NH_2 , and CH_3I , for MAPbI_3 and $\text{MAPbI}_3 + \text{SnO}_2$. Reproduced with permission.^[33] Copyright 2020, American Chemical Society.

This article is protected by copyright. All rights reserved.

4.2. Chemical Reaction

The SnO₂ itself is relatively stable under thermal, pressure, and bias stress. However, the SnO₂ ETL is in direct contact with the perovskite layer in an n-i-p PSC. Reactions between metal oxides and perovskite have been previously reported, where the metal oxides (e.g., TiO₂, NiO_x, and SnO₂) can react with perovskite and cause decomposition of the organic cation at the interface.^[33, 90] SnO₂ can also react with perovskite because of its catalytic properties from the exposed facet and active defects on the surface under exterior stresses. Although SnO₂ is less photocatalytic than TiO₂, it is not perfectly harmless to perovskite under UV illumination.^[89, 91, 92] In particular, the weak Pb-I bond in I-based perovskite (e.g., MAPbI₃) is delicate, and contacting SnO₂ with perovskite can lead to perovskite degradation to PbI₂ (**Figure 4c-d**).^[89] Thampy *et al.* reported the interfacial reaction between an oxide transport layer (TiO₂, SnO₂, and NiO) and MAPbI₃ under thermal stress.^[33, 93] Because of an acidic hydrolysis reaction, the interfacial degradation of MAPbI₃ in contact with SnO₂ produces H₂O, CH₃NH₂, PbI₂, and SnI₄ at a lower temperature than that of degradation of MAPbI₃ by itself (**Figure 4e-f**). The decomposition reaction pathways and phase stability are different depending on perovskite composition and aging condition, and direct contact between SnO₂ and perovskite can cause unpredictable degradation and unsettled stability in full devices during operation. Therefore, efforts on interfacial engineering and surface modification are crucial for PSC research.

4.3. Mechanical Properties

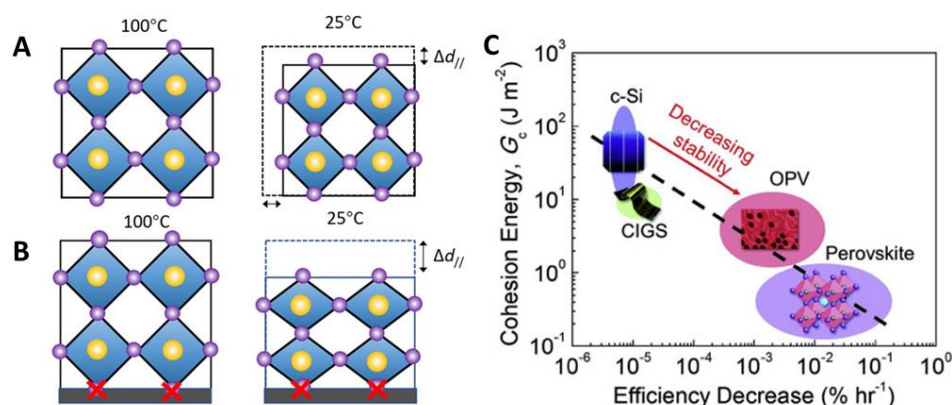


Figure 5. a-b) Schematic illumination of the strain formation process without substrate (a) and with substrate adhesion (b). Reproduced with permission.^[94] Copyright 2019, Nature Publishing Group. c) The measured cohesion, G_c , and efficiency decrease as a function of solar cell active material, showing a correlation between mechanical integrity and long-term reliability. Reproduced with permission.^[95] Copyright 2017, Wiley-VCH.

Accepted Article

Because PSCs are made of multiple stacking layers with vastly different mechanical properties, it is important to understand the potential of an adhesive and cohesive failure during device fabrication and operation. Because the perovskite layer has higher thermal expansion coefficients than other device layers and the glass substrates, the perovskite layer is prone to developing residual stresses during processing.^[83, 94, 96, 97] Thermally induced tensile stresses in a perovskite film can be caused by the lattice mismatch and different thermal expansion coefficients of different layers in a device stack during the perovskite deposition at an elevated temperature (**Figure 5a-b**).^[94] Rolston *et al.* showed that the adhesive and cohesive fracture resistance (G_c) of PSCs is relatively low ($\sim 1.5 \text{ J/m}^2$) in comparison to other types of solar cells, such as organic photovoltaic, Si photovoltaics, and copper indium gallium selenide solar cells (**Figure 5c**); thus, PSCs are generally fragile and susceptible to delamination.^[95] The low G_c value and toughness of perovskite would result in accumulating residual stress and inducing fracture in perovskites. To release the stress in the perovskite layer and increase the mechanical robustness of PSCs, a buffer layer such as polystyrene and surface modification with self-assembled molecules (SAMs) was introduced at the SnO_2 /perovskite interface to improve stability. We discuss more details on some strategies for improving the mechanical properties to increase PSC efficiency and stability in Sections 5 and 6.

5. SnO_2 Modification for High-Performance PSCs

Although SnO_2 has shown general advantages as an ETL in PSCs, it still suffers from some issues, as mentioned in previous sections. Like many other semiconducting oxides, the SnO_2 film also contains defects inside the bulk crystals as well as on the film surface. Modulating these defects strongly affects electron extraction and injection, which is shown to be critical for improving device efficiency and stability. In this section, we discuss two main strategies—bulk crystal modification and interface engineering—commonly reported in the literature.

5.1. Bulk Crystal Modification Using Doped SnO_2

The electronic properties of the ETL can greatly affect charge carrier dynamics and device characteristics. The energetics at the ETL/perovskite interface can facilitate charge separation to minimize interfacial recombination losses. Tailoring the Fermi level and/or charge mobility is often utilized to tune ETLs to be a good selective contact with perovskite.

The Fermi level, which is correlated to the free electron concentration, can be modulated with doping with metallic or nonmetallic elements. Doping metal oxides is an effective method to control the band offset, Fermi level, and electrical conductivity, reducing the contact resistance and

This article is protected by copyright. All rights reserved.

Accepted Article

recombination at the ETL/perovskite interface.^[52] In the absence of additional extrinsic elements, SnO₂ often exhibits self-doping via intrinsic defects such as Sn_i and V_o, which are dominant defects during SnO₂ synthesis; however, it is difficult to control self-doping with good reliability and reproducibility.^[98] In contrast, doping SnO₂ with extrinsic ions such as metal cations and/or halide ions have been successfully demonstrated. So far, doping SnO₂ with Li(1⁺), Mg(2⁺), Al(3⁺), Ga(3⁺), Y(3⁺), Nb(5⁺), and Sb(5⁺) has been used to form Sn_i and V_o with various amounts and ratios, leading to increased n-type conduction.^[15, 98, 99] Among them, Li⁺ doping is the most effective for improving the charge dynamics in the SnO₂ ETL.^[99, 100]

Doping SnO₂ with halogen ions (e.g., Cl⁻ and F⁻) has also been studied for improving surface passivation and band alignment.^[101-104] This halogen-doping-based strategy can improve the charge transport layer with better refractive index and absorbance, as well as reduced number of defects with suppressed charge carrier accumulation near the SnO₂/perovskite interface region. Thus, the alkali-halogen-salt treatment of SnO₂ has been commonly adopted for passivating defects at the SnO₂/perovskite interface.^[25, 105, 106] Note that some halogen dopants can increase the photocatalytic activity compared to bare SnO₂ because the interstitial and substitutional halogen ions in SnO₂ could create gap states from the hybridization of O-2p with halogen 1s orbitals.^[101]

5.2. SnO₂ Surface Modulation and Interface Engineering

Beyond the bulk properties of the SnO₂ ETL film, the surface condition and interaction between ETL and perovskite also affect the efficiency and/or stability of PSCs. Although SnO₂ has unique intrinsic features as an ETL, the surface defects and dangling bonds can form during SnO₂ preparation, causing unwanted recombination and degradation pathways.^[34, 107-109] Because perovskite crystals grow atop the ETL, the surface conditions of ETL can influence the quality and stability of the perovskite film, as well as the adhesion and interaction at the perovskite/ETL interface. To date, numerous strategies have been developed for minimizing the charge carrier recombination and improving the interfacial energy level alignment and electronic coupling. Here, we discuss some effective surface modification and interface engineering techniques reported in the literature.

5.2.1. Ionic Salts

Ionic salts can effectively passivate the charged (positive and negative) surface defects such as hydroxyl groups, oxygen vacancies, exposed Sn atoms, and dangling bonds through hydrogen bonding and electrostatic interaction.^[25, 106] Moreover, cations and/or anions from the salts can not only be nucleus sites for perovskite formation by strong ionic bond with perovskite precursor, but also simultaneously passivate the defects of perovskite by ion exchange or ion diffusion into the perovskite

This article is protected by copyright. All rights reserved.

layer. For the SnO₂ layer in n-i-p-structured PSCs, alkaline halide salts (e.g., KCl, KF, and RbF) and ammonium halide salts (e.g., NH₄Cl and NH₄F) are commonly used for SnO₂ surface modulation.^[25, 103, 105, 110-112]

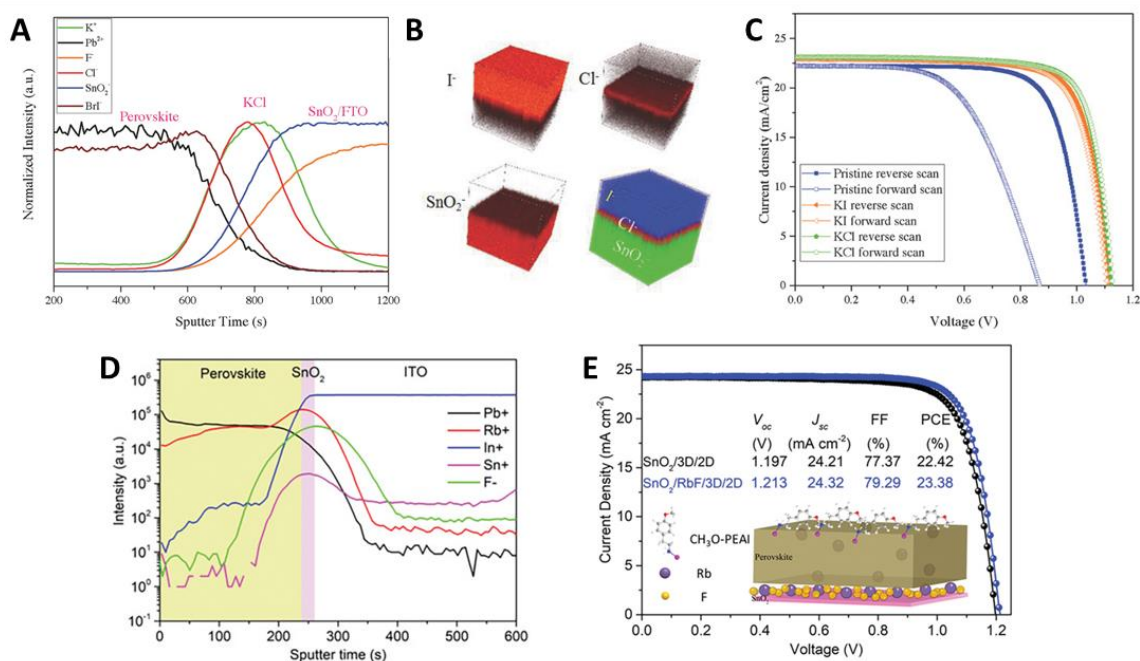


Figure 6. a-b) Depth profile of the KCl, which remained at the SnO₂/perovskite interface, confirmed by secondary-ion mass spectrometry (SIMS). a) Normalized SIMS results of the complete perovskite film on substrates treated by KCl solution. b) 3D render overlay of I⁻, Cl⁻, and SnO₂ SIMS data. c) *J*-*V* curves of PSCs with SnO₂ passivation materials of KI and KCl. Reproduced with permission.^[106] Copyright 2018, Wiley-VCH. d) Time-of-flight secondary-ion mass spectroscopy (ToF-SIMS) depth profile of the ETL/RbF/perovskite structure. e) *J*-*V* curves of champion PSCs based on SnO₂ and SnO₂/RbF. Reproduced with permission.^[105] Copyright 2021, Wiley-VCH.

Liu *et al.* studied the passivation effect of KCl and identified that the K/Cl ions can passivate the ETL/perovskite interface.^[106] The K and Cl ions were located at the ETL/perovskite interface and were not incorporated in the perovskite lattice (**Figure 6a-b**).^[106] This result is consistent with another study by Bu *et al.*, where K ions were found at the grain boundaries, passivating defects and reducing nonradiative recombination.^[72] SnO₂-based PSCs with the KCl passivation layer showed substantial enhancement of the average V_{oc} owing to reduced interfacial trap density and increased carrier lifetime (**Figure 6c**).^[25] Similarly, Jung *et al.* used ammonium fluoride (NH₄F) as a bifunctional surface passivator to reduce the defect density and adjust the Fermi level of SnO₂.^[112] With NH₄F, the

This article is protected by copyright. All rights reserved.

ammonium ions (NH_4^+) can suppress the surface hydroxyl groups, and the fluorine ions (F^-) can substitute into the defect site (i.e., bridge-hydroxyl), leading to reduced energy losses and improved efficiency of PSCs. In another study, Zhuang *et al.* showed SnO_2 surface engineering with RbF either by mixing into SnO_2 precursor or via post-treatment on the SnO_2 surface.^[105] When RbF is applied to the SnO_2 layer during the post-treatment, the active Rb^+ cations can be incorporated in the bulk perovskite grain, leading to suppressed ion migration in perovskite as well as reduced recombination at the SnO_2 /perovskite interface (**Figure 6d**). Finally, PSCs with double-sided passivation using RbF and CH_3O -phenethylammonium iodide (PEAI) on the SnO_2 and perovskite surface, respectively, produced an outstanding PCE of 23.38% with a V_{oc} of 1.213 V, corresponding to a small V_{oc} deficit of only 0.347 V (**Figure 6e**). Overall, these and other reported ionic salts (e.g., KF , NH_4Cl , and ethylene diamine tetraacetic acid [EDTA]-K) have been selected for targeting simultaneous passivation of both positively and negatively charged defects. Although they show similar effects, KCl treatment seems more effective and is commonly used nowadays.

5.2.2. Functional Organic Compounds

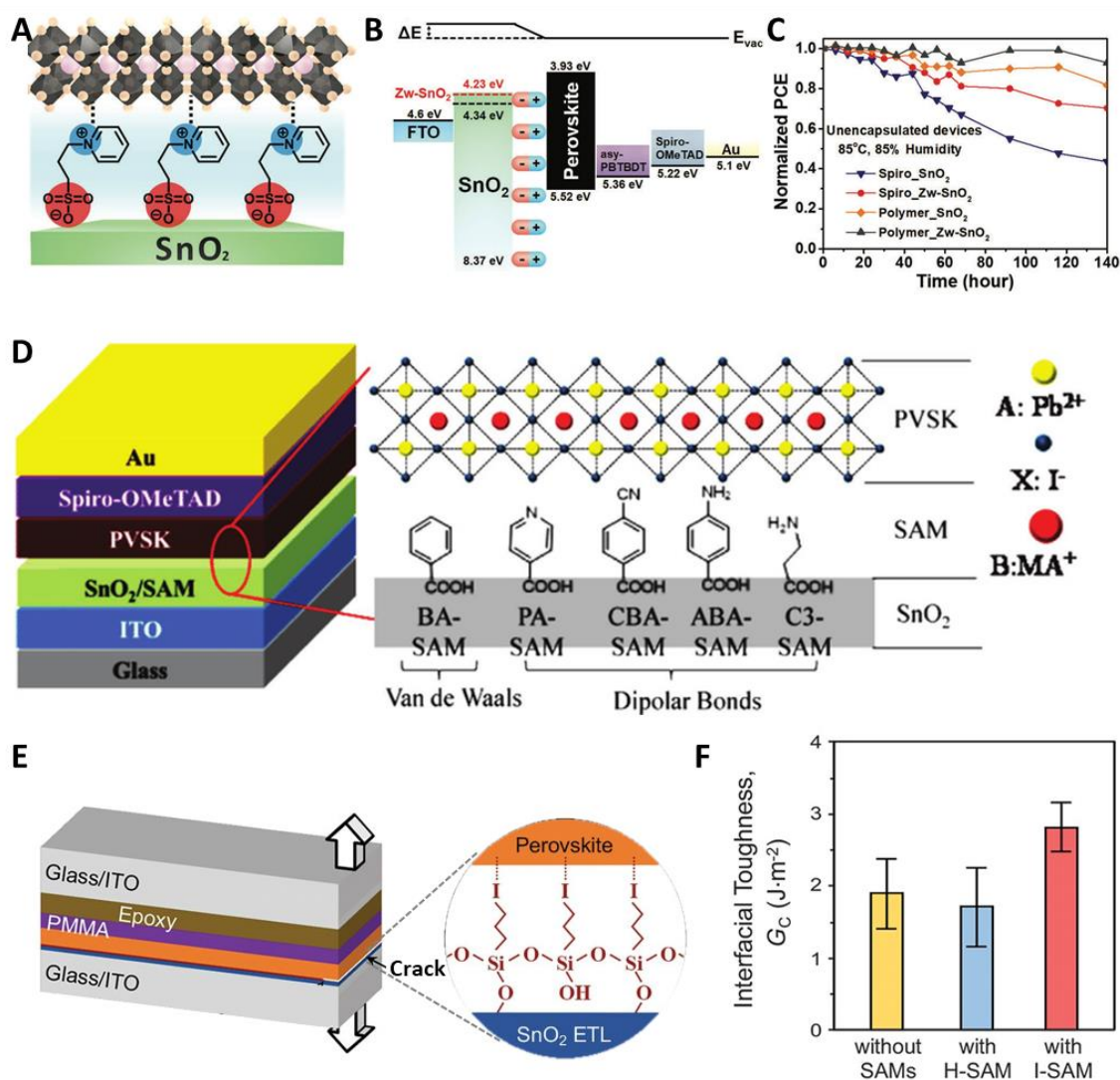


Figure 7. a-c) Schematic illustration of the formation of a zwitterionic compound, 3-(1-pyridinio)-1-propanesulfonate, on the SnO₂ layer (a), energy diagram of each layer of the corresponding device (b), and comparison of device stability at 80°C and 85% RH (c). Reproduced with permission.^[107] Copyright 2018, Royal Society of Chemistry. d) Schematic illustration of tuning the SnO₂/perovskite interface with various SAMs. Reproduced with permission.^[113] Copyright 2017, American Chemical Society. e-f) Mechanical behavior of the ETL/perovskite interface with I-SAM (e), and comparison of toughness of ETL/perovskite without SAMs and with SAMs (H-SAM or I-SAM) (f). Reproduced with permission.^[114] Copyright 2021, American Association for the Advancement of Science (AAAS).

The terminal functional groups in organic compounds can directly interact with the Sn or O dangling bonds on the SnO₂ surface and form a permanent dipole moment, shifting the Fermi level and conduction band.^[107] Organic compounds with mixed charged functional groups—such as SAMs and zwitterionic organic compound (ZwCs)—have been used to bond the SnO₂ layer to perovskite

This article is protected by copyright. All rights reserved.

layer to passivate SnO₂ with better interfacial optoelectronic properties.^[34, 108, 113, 114] ZwCs contains both negatively and positively charged functional groups. In general, the negatively charged groups such as -COO⁻ and -SO₃⁻ anions bond with SnO₂ through the ester and chelate bonds, whereas the positively charged group such as -NH₃⁺ cation interacts with halide anion in perovskite through electrostatic attractions. The interfacial chemical bridges associated with zwitterions can reduce contact defects and realign interfacial energy levels for better device operation and stability. For instance, 3-(1-pyridinio)-1-propanesulfonate as a ZwCs was utilized to modulate the SnO₂ ETL surface as shown in **Figure 7a-b**.^[107] This ZwCs-modified SnO₂ layer in PSCs showed desirable properties, including high conductivity, effective charge extraction, and large recombination resistance. In addition, the -NH₃⁺ cation in ZwCs was shown to passivate Pb-I antisite defects and reduce trap states of perovskite. The ZwCs-SnO₂-based PSC with dopant-free HTL achieved a PCE of 20.5% with improved V_{oc} and stability under 85°C and 85% relative humidity (RH) (**Figure 7c**).

Like ZwCs, SAMs also contain multiple functional groups, including the head group (surface-reactive functional group), tail group (low-surface-energy functional group), and alkyl chain.^[113] The head groups normally covalently bind to metal oxide surface through chelating or anchoring groups such as silanes, amines, phosphonates, and carboxylates. The tail groups can be exposed and reconfigure the surface properties and react with the perovskite layer. To date, various SAMs have been utilized to modify the SnO₂ surface. Examples of SAMs include benzoic acid, 3-aminopropyltriethoxysilane, 4-pyridinecarboxylic acid, 3-aminopropanoic acid, 4-aminobenzoic acid, and 4-cyanobenzoic acid (**Figure 7d**). Overall, SAMs with carboxylates and silane head groups have been mostly studied for SnO₂-based PSCs.^[113] Zuo *et al.* showed that SAMs with carboxylic acid functional groups can interact with both tin and oxygen dangling bonds on the SnO₂ surface and passivate the SnO₂ surface with high coverage.^[113] On the other hand, modifications based on SAMs with different terminal functional groups (tail groups) showed different trends compared to that of the work function variation. These abnormal phenomena were attributed to the strong chemical interactions between perovskite and SAMs with their terminal functional groups. Pyridine could passivate SnO₂/perovskite interface and lower the work function of SnO₂, so the device with the 4-pyridine carboxylic acid modification showed significant improvement in electronic coupling at the SnO₂/perovskite interface.^[113]

SAMs consisting of silane also have been used to enhance device efficiency and stability through passivation of defects and enhanced interfacial adhesion.^[115] Yang *et al.* reported that SnO₂ with a silane-based SAM (3-aminopropyltriethoxysilane) can provide better surface wetting property, resulting in more intimate contact between SnO₂ and perovskite with improved perovskite

This article is protected by copyright. All rights reserved.

morphology.^[116] The silane groups also passivate the defects by reacting with -OH groups on SnO₂, leading to a lower defect concentration and charge recombination. In another recent study, Dai *et al.* showed that the I-terminal SAM (I-SAM) can be applied to strongly strengthen the interface; the silane head group can be cross-linked with SnO₂ through the salinization process, and the I terminal group strongly bonds to perovskite by the non-covalent interaction (**Figure 7e-f**).^[114] The strong halogen bonding at the interface can enhance the average interfacial adhesion toughness by about 50% compared to that of using H-terminal SAM (H-SAM), with improved device efficiency and stability.

Overall, bifunctional organic compounds such as ZwCs and SAMs are highly effective for enhancing both PCE and stability. The application process for the bifunctional organic compounds is simple, reproducible, and attractive for scaling up PSCs.

5.2.3. SnO₂-Based Bilayer ETL Structure

A bilayer approach by combining the SnO₂ layer with another bulk layer (e.g., a different metal oxide, bulk polymer, carbon, or fullerene derivatives) has also shown promise for improving SnO₂ ETL.^[13, 81, 117-120] Unlike other surface engineering methods discussed previously—such as oxygen treatment and surface modulation using ionic salts and functional groups—the approach based on a combination of different layers was primarily to increase the compactness and overall conductivity of the ETL. The bulk layer surface coating can also passivate the SnO₂ surface with reduced recombination and energy loss, improving PSC efficiency and operational stability. For example, Dagar *et al.* introduced a thin MgO overlayer on SnO₂ layer to achieve uniform films, which reduced interfacial carrier recombination and led to better stability.^[120] Red-carbon quantum dots, one of the carbon derivatives, can be used to fabricate the carbon/SnO₂ composite ETL to provide efficient charge collection and better electron extraction. PSCs based on SnO₂ ETL incorporated with red-carbon quantum dots, although not technically a bilayer structure, achieved a PCE of 22.77% with shelf life up to 1,000 h (dark condition, 40% RH).^[117]

Bulk polymer and fullerene derivatives generally play a similar role as SAMs by forming an ultra-thin layer at the ETL/perovskite interface. Notably, some conductive polymers such as fullerene derivatives (like C₆₀-SAMs) and PCBM can enable good electron extraction from the perovskite layer with high electron affinity.^[121, 122] In contrast, non-conductive polymers such as poly(ethylene glycol) and poly(ethylenimine) ethoxylated should form a thin layer with fine adjustment of the optimum thickness, which can cause a reproducibility issue and large contact resistance.

Inorganic materials as the second layer combining with the SnO₂ ETL have also attracted research interest for providing pinhole-free and dense ETL with favorable band alignment. Several

This article is protected by copyright. All rights reserved.

metal oxide bilayers such as ZnO/SnO₂, SnO₂/MgO, and SnO₂/TiO₂ showed enhanced device performance via substantial reduction of the recombination rate at the ETL/perovskite interface.^[123-126] Nonetheless, since SnO₂ is already a better ETL material than most other metal oxides, potential detrimental effects from the second inorganic layer should be considered. For example, TiO₂ has the UV stability issue, ZnO's high reactivity associated with residual hydroxyl groups and acetate ligand on the surface can lead to the stability issue,^[126-129] and a thick MgO layer may increase charge transfer resistance due to its insulating properties.

A related and more recent strategy is to form an atomic-level interlayer that can interconnect/react at the SnO₂/perovskite interface and provide interfacial passivation.^[31, 130] It is expected that some reactions may occur when halogen-bonded SnO₂ and perovskite precursor are in contact because of spontaneous exchange between the halogen ions from the SnO₂ surface and perovskite precursor. In addition, SnO₂ can hold a large number of Cl⁻ ions—occupying the O-vacancy sites and O sites—which can facilitate spontaneous reactions to form the atomic interlayer. However, it is difficult to obtain evidence to verify the formation of atomically coherent interlayer at the SnO₂/perovskite interface. Most recently, Min *et al.* reported the formation of a coherent interlayer between a SnO₂ and a perovskite layer, achieved by coupling Cl-bonded SnO₂ with a Cl-containing perovskite precursor.^[31] In this study, several atomic-level characterizations collectively imply the formation of a crystalline FASnCl_x-based atomically coherent interlayer between SnO₂ and perovskite, and this interlayer reduces interfacial defects and enhances charge extraction from the perovskite layer, enabling the demonstration of a PSC with PCE of 25.8% (25.5% certified).

6. Stability of SnO₂-Based PSCs

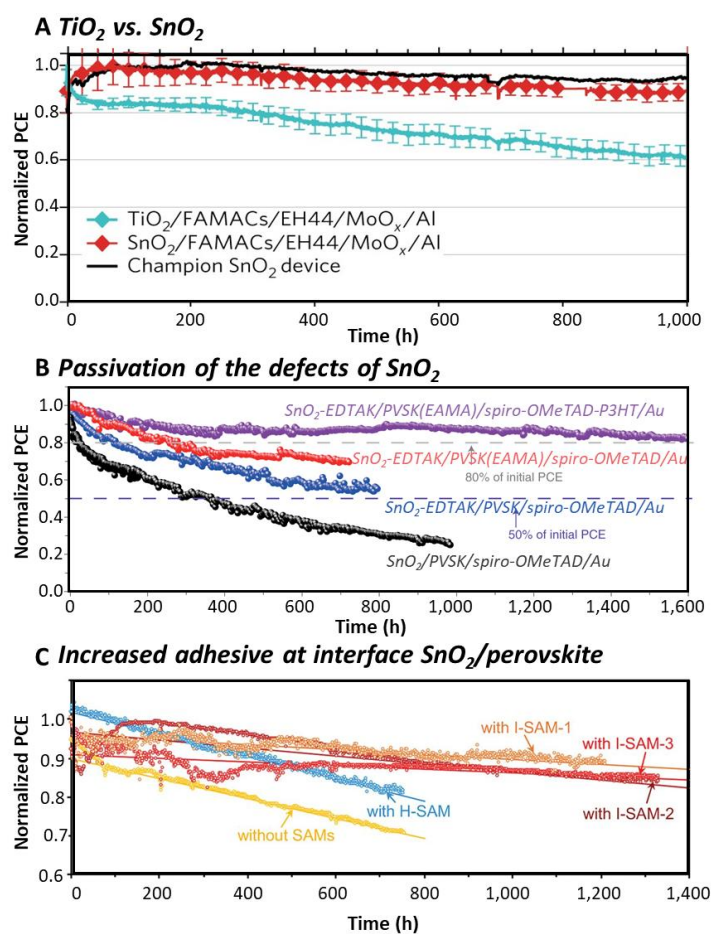
Although PSC technology development has been tremendous during the past decade, long-term operational stability remains the main concern for market entry of PSCs. To improve the stability of PSCs, many factors need to be considered and improved, including the phase stability of each device layer; the resistance, adhesion, and chemical reaction at the interface; and influence from the external environment. In addition to ETL-related instability issues, the key matters that can result in degradation of PSCs over time are correlated with temperature increase and unbalanced interfacial charge dynamics during solar cell operation.

In the relationship between ETL material and contact stability, TiO₂ is a well-known photocatalyst and can lead to perovskite decomposition to PbI₂ under UV light exposure.^[126, 127] In addition, ZnO generally has abundant hydroxyl groups on the surface, and it can cause deprotonation

This article is protected by copyright. All rights reserved.

of perovskites, especially under thermal stress.^[129] Such photo- and thermal-reactivities of metal oxides in PSCs usually lead to poor long-term operational stability, and thus proper alternatives or mitigating strategies should be developed.

Several studies have shown that SnO₂ is a suitable ETL for improving the operational stability of PSCs. As shown in **Figure 8a** for a stability comparison of TiO₂ and SnO₂ ETL in n-i-p PSCs, the SnO₂-based devices showed much better operational stability than TiO₂-based devices, retaining over 94% of initial PCE after 1,000 h.^[32] However, as aforementioned, the hydroxyl groups and oxygen defects are present on the SnO₂ surface and can induce perovskite degradation near the SnO₂/perovskite interface. Therefore, by eliminating the hydroxyl groups and passivating the SnO₂ surface, the stability of PSCs can be further improved.^[38] Liu *et al.* reported a holistic interfacial stabilization strategy—combining modifications to the ETL (SnO₂/EDTA-K), perovskite layer, and HTL—which lead to demonstration of unencapsulated perovskite solar modules with a T₈₀ lifetime of over 1,600 h (**Figure 8b**).^[38]



This article is protected by copyright. All rights reserved.

Figure 8. a) Stability comparison of PSCs based on a stack of ETL/perovskite/9-(2-ethylhexyl)-N,N,N,N-tetrakis(4-methoxyphenyl)-9H-carbazole-2,7-diamine (EH44)/MoO_x/Al in which the ETL layer is either TiO₂ or SnO₂ at room temperature in ambient. The best stability for a SnO₂-based device is shown as a black line. Reproduced with permission.^[32] Copyright 2018, Nature Publishing Group. b) Operational stability of non-encapsulated perovskite solar modules with varying structures biased near the initial MPP under 1-sun illumination in N₂ with <5% RH. Reproduced with permission.^[38] Copyright 2020, Nature Publishing Group. c) Comparison of operational stability of unencapsulated PSCs without and with H-SAM or I-SAM by MPP tracking under 1-sun illumination, in N₂, at room temperature. Reproduced with permission.^[114] Copyright 2021, American Association for the Advancement of Science (AAAS).

The mismatch of mechanical properties and insufficient adhesion between the ETL and perovskite can drive premature delamination and fracture under internal and external mechanical stresses. Thus, enhancing the adhesion or toughness between the ETL and perovskite in a complete device stack can improve the overall device performance and stability. Very recently, I-SAM has been utilized as a molecular glue to strengthen the toughness of the SnO₂/perovskite interface, which improved device stability under maximum-power-point (MPP) operation, retaining >80% of initial PCE up to about 4,000 h (**Figure 8c**).^[114]

There are multiple pathways for how the performance of PSCs can degrade over time, and it is usually difficult to deconvolute the effects from various factors, such as the charge transport layers, perovskite layer, and metal ion diffusion from dopant and metal electrodes. However, it is safe to say that SnO₂ is currently one of the best candidates as the ETL in n-i-p-structured PSCs with promising operational stability; further improvements can be expected by utilizing advanced interface/bulk engineering strategies.

7. Scaling Up and Flexible Devices

7.1. Large-Area Module

When PSCs are scaled up to larger substrates, the photovoltaic performance significantly decreases, primarily because of the increased series resistance and nonuniformity of device layers.^[131-133] Most research efforts on the module development have focused on module design (sub-cell dimensions and gap between two adjacent sub-cells), laser/mechanic scribing conditions, and engineering large-area perovskite thin films with good uniformity and quality (e.g., minimum defects, large grains, and smooth surface).^[71, 72, 132] Since most of the advances are developed based on spin-

This article is protected by copyright. All rights reserved.

coating methods for small-area PSCs and are not easily transferable to module fabrication, other scalable coating methods such as slot-die, bar coating, blade coating, spray-coating, and screen printing should be developed.^[71, 132, 134-137]

To utilize the SnO₂ ETL for large-area modules, it is critical to prepare pinhole-free and uniform SnO₂ films over the entire substrate area, including the scribing area. Spin-coating is the simplest and most developed method for fabrication of thin films for small-area PSCs. Spin coating has also been used for exploring SnO₂ precursors for module fabrication. Jung *et al.* showed an electrostatic self-assembly method for colloidal SnO₂ solution (SA-SnO₂) for coating a conformal and uniform SnO₂ ETL on a large-area substrate (**Figure 9a**).^[137] The uniform SA-SnO₂ thin film is successfully formed on 25-cm² FTO substrate with reduced shunt resistance, and a corresponding electroluminescence image is shown in **Figure 9b**. Finally, a SnO₂-based min-module was demonstrated with PCEs of 15.3% and 14% with 25- and 100-cm² substrates, respectively. Although spin coating was used in this study, the reported self-assembly approach for SnO₂ deposition is expected to also be suitable for other scalable deposition methods.

This article is protected by copyright. All rights reserved.

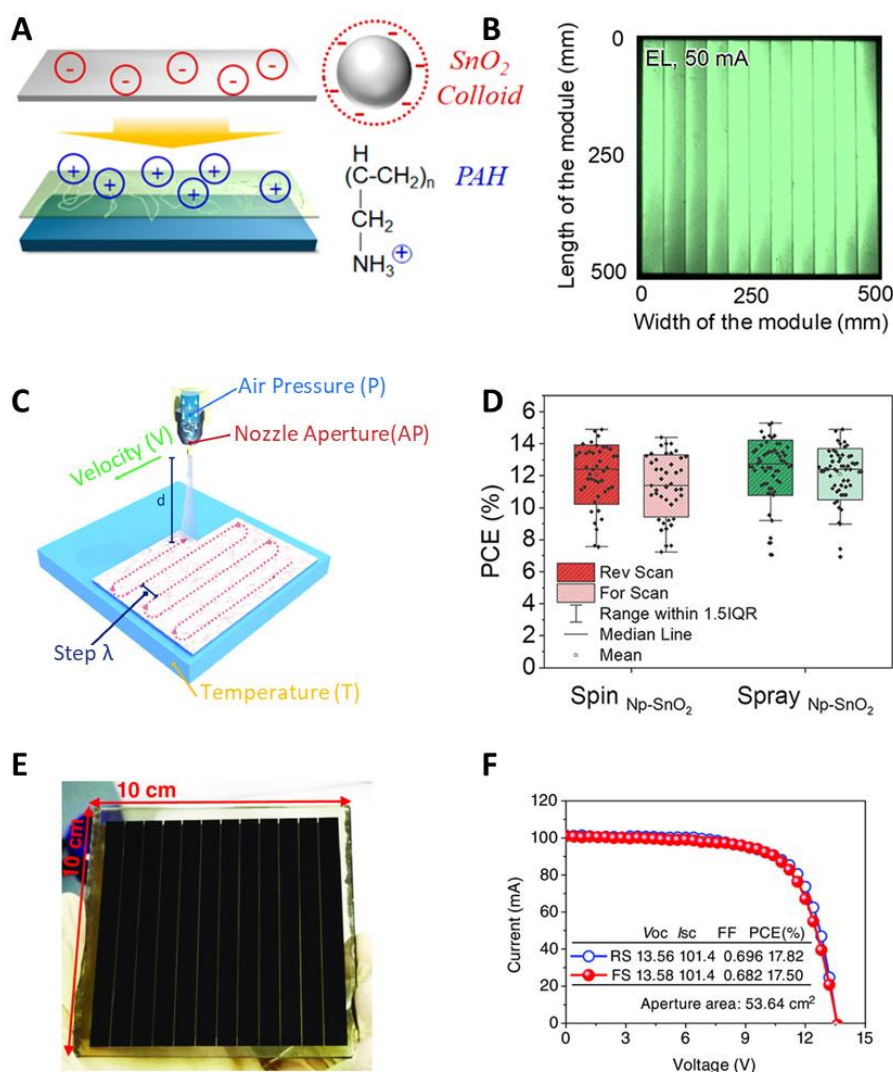


Figure 9. a-b) Illustration of the electrostatic self-assembly SnO_2 colloidal on a substrate by charge attraction at the surface between the positively charged FTO/poly(allylamine hydrochloride) (PAH) and negatively charged SnO_2 colloids (a), and the corresponding electroluminescence data of SA- SnO_2 based mini-module (b). Reproduced with permission.^[137] Copyright 2019, American Chemical Society. c) Schematic image of SnO_2 deposition with an automated spray coating (ASC). Reproduced with permission.^[134] Copyright 2020, Wiley-VCH. d) Statistical comparison of PCEs of spin-coated and spray-coated SnO_2 -based PSCs. Reproduced with permission.^[71] Copyright 2021, American Chemical Society. e-f) Photograph of the $10 \times 10 \text{ cm}^2$ perovskite solar module based on ITO/CBD SnO_2 /perovskite (e), and the corresponding certified PCE of 17.4% for the perovskite solar module with $10 \times 10 \text{ cm}^2$ substrate (f). Reproduced with permission.^[138] Copyright 2019, Wiley-VCH.

Colloidal SnO_2 NP-based precursor ink is suitable for scalable deposition (e.g., slot-die and spray coating) for preparing large-area SnO_2 films. Bu *et al.* showed a general KOH treatment to SnO_2

This article is protected by copyright. All rights reserved.

is critical for obtaining high-performance devices, including small planar cells, flexible cells, and modules based on slot-die-coated SnO₂ ETL.^[72] Taheri *et al.* developed a simple and scalable deposition approach based on automated spray-coating (ASC) to prepare uniform and dense SnO₂ ETLs (**Figure 9c-d**).^[71, 134] They showed that the small-area PSCs based on ASC-SnO₂ and spin-coated SnO₂ ETLs had comparable device performance. In a follow-up study, the ASC method was further utilized to prepare uniform and dense SnO₂ ETL over a large-area substrate, leading to demonstration of modules with PCE of 12% and 10.7% with 16.84- and 21.2-cm² active areas, respectively.^[71]

The CBD method for SnO₂ deposition has also been tested for preparing modules because it is useful to achieve uniform and large-area thin film.^[35, 73, 138] Bu *et al.* used CBD SnO₂ ETL in a demonstration of a perovskite module with a 53.64-cm² active area with a certified PCE of 17.4% (**Figure 9e-f**).^[138] Recently, Tong *et al.* introduced KMnO₄ as an additive to CBD precursor to prepare the SnO₂ layer over a large area. The high-oxidant property of KMnO₄ promotes the complete oxidation of the SnCl₂ precursor and provides additional K and Mn ions on the SnO₂ film to improve the quality of perovskite films.^[35] In this study, perovskite modules with 22.4- and 91.8-cm² active areas showed PCEs of 17.26% and 13.72%, respectively; an encapsulated 5×5-cm² module showed less than 20% degradation over 1,000-h operation in ambient condition.

The research for scaling up small-area devices to modules is essential for commercialization of PSCs. Various factors—such as the manufacturing costs, intrinsic stability, and reproducibility—should be carefully considered when developing scalable SnO₂ deposition methods for efficient and stable perovskite modules.

7.2. Flexible Solar Cells

The low-temperature fabrication requirement for SnO₂ has made it suitable for flexible PSC development. Since the commonly used flexible plastic substrates—such as polyethylene terephthalate (Tg: 70°C–110°C) and polyethylene naphthalate (PEN) (Tg: 120°C–155°C)—can only endure <150°C thermal stress, much research for flexible PSCs has focused on the low-temperature fabrication and modification methods for SnO₂ deposition.^[139] To reduce the post-annealing temperature, as-synthesized SnO₂ colloidal precursor has been considered as an efficient way to form the ETL.^[56, 139] SnO₂ nanocrystals have been synthesized by several different methods, including hydrolysis, hydrothermal method, hot-injection method, and inverse micelle-water injection method.^[15, 56, 140, 141] For example, Park *et al.* demonstrated the coating of uniform and dense SnO₂ ETL on flexible ITO substrate by using the pre-synthesized SnO₂ quantum dots dispersed in a nonpolar solvent followed by annealing at 80°C to facilitate solvent evaporation.^[56] The champion flexible PSCs

This article is protected by copyright. All rights reserved.

achieved a PCE of 17.7% with J_{sc} of 19.7 mA/cm², a V_{oc} of 1.13 V, and an FF of 0.79, which is comparable to the performance of PSCs on the rigid ITO substrate.

Besides solution deposition method, plasma-enhanced ALD is one of the representative low-temperature deposition methods for growing the compact and thin oxide film. However, even though the oxygen plasma and ozone source can enable SnO₂ layer formation at a low temperature, residual impurities and defects exist in the SnO₂ layer. These issues result in low V_{oc} , FF and high hysteresis in J - V curve; post annealing treatment at high temperature is necessary to remove the impurities and improve the conductivity.^[66, 74] In one study, Wang *et al.* reported the water vapor treatment of plasma-enhanced ALD-SnO₂ at 100°C to form a purer SnO₂ with complete reaction of all organic materials.^[142] It was found that the water-vapor-treated SnO₂ film improved the electrical conductivity of SnO₂ ETLs, leading to flexible PSCs with a PCE of 18.36% (17.12%) measured under reverse (forward) voltage scan and a stabilized PCE >17%.^[142] Note that the aforementioned surface treatment strategies (Section 5) and scalable deposition methods (Section 7.1) can all be applied to flexible PSCs and modules. For example, EDTA-SnO₂ and KOH modification on SnO₂ was used in flexible PSCs with PCE >18%.^[28] Similarly, Bu *et al.* obtained a PCE of 15.22% for a flexible perovskite module (5×6 cm²) using KOH-treated Alfa-SnO₂ film by slot-die coating.^[72]

In addition, unlike the perovskite layer and organic material layer, which are relatively flexible materials, the inorganic SnO₂ layer is stiff and robust. These different mechanical properties and the weak adhesion at the SnO₂/perovskite interface is vulnerable under repeated bending fatigue.^[83, 84] In this regard, there are significant ongoing efforts to understand the mechanical characteristics and make high-endurance flexible PSCs under repeated cyclic-bending operation. Recently, Dong *et al.* used an FAI-incorporated SnO₂ (FI-SnO₂) ETL to obtain an interpenetrating perovskite/ETL interface with enhanced structural integrity.^[143] In this study, a PCE of 20.1% was obtained under reverse J - V scan direction, with J_{sc} of 22.4 mA/cm², V_{oc} of 1.15 V, and FF of 0.782; under forward scan, the PCE was 19.6%, with J_{sc} of 22.4 mA/cm², V_{oc} of 1.14 V, and FF of 0.769 (**Figure 10**). As seen in **Figure 10**, after 1,000 bending cycles, the perovskite film began to peel off from the pristine SnO₂ ETL, while the FI-SnO₂ perovskite/ETL interface showed virtually no morphological changes. When the bending cycle reached 2,500, the pristine perovskite/SnO₂ film showed a more obvious delamination phenomenon, whereas the perovskite/FI-SnO₂ interface was still largely intact.

This article is protected by copyright. All rights reserved.

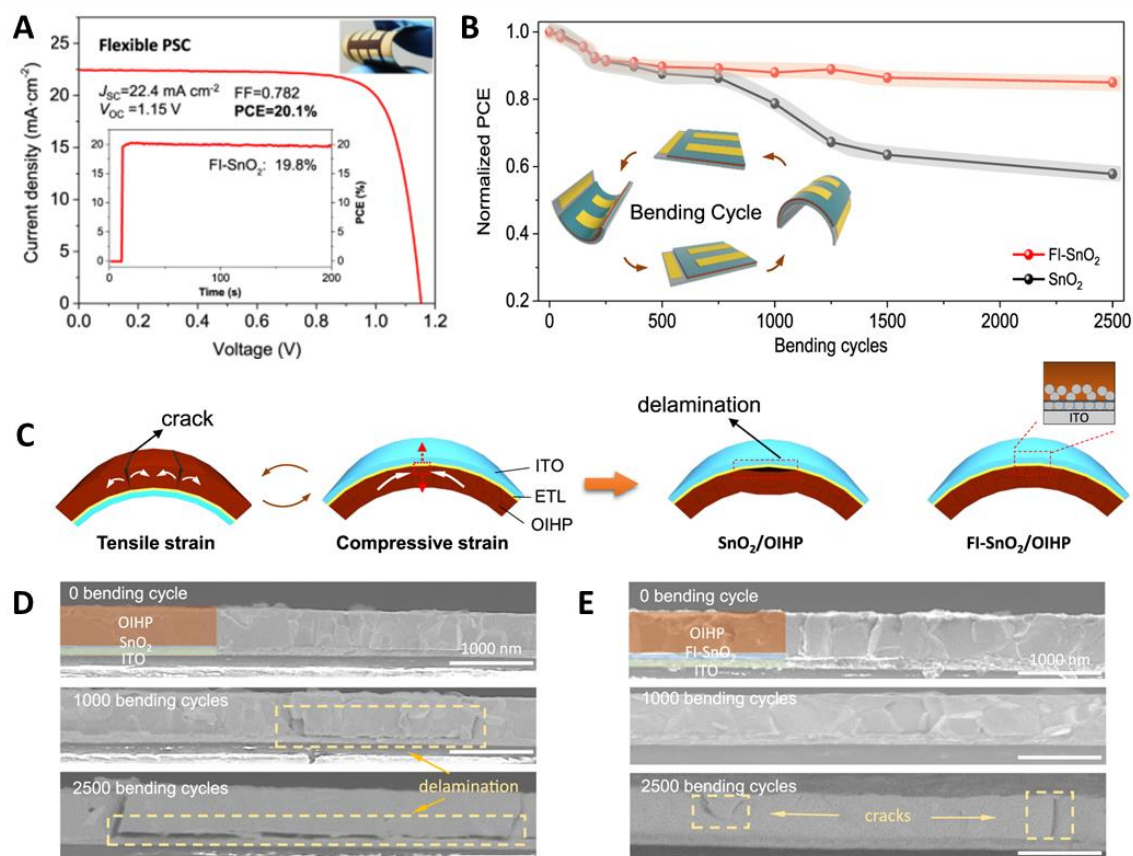


Figure 10. a) J - V characteristics and MPP tracking of flexible PSCs based on FI-SnO₂ ETL. b) Durability comparison of flexible PSCs based on FI-SnO₂ and pristine SnO₂ ETLs as a function of mechanical bending cycles (40% RH; ambient air; 25°C; 3-mm minimum bending radius). c) Schematic illustrations showing the strains in perovskite layers under different bending states (left panel) and the film states after bending cycles (right panel). d-e) Cross-section scanning electron microscope images of flexible PEN/ITO/SnO₂/perovskite film (d) and PEN/ITO/FI-SnO₂/perovskite film (e) after different bending cycles. Reproduced with permission.^[143] Copyright 2021, Nature Publishing Group.

8. Challenges and Strategies for Further Advances of SnO₂

Although SnO₂-based n-i-p PSCs have reached a PCE level that is competitive to other mature photovoltaic technologies, significant hurdles exist for their commercialization in the future. Since the conventional preparation method for TiO₂ ETL generally includes the post-annealing at 450–500°C to obtain the crystalline TiO₂ and remove the residual organic materials, there were not many unpredictable variables on the surface of the TiO₂ ETL. In contrast, almost all SnO₂ ETLs prepared from various methods have been developed based on low-temperature annealing treatment, mostly lower

This article is protected by copyright. All rights reserved.

than 180°C, which is below the normal temperature for obtaining crystalline SnO₂ along with removal of the hydroxyl groups and/or organic residuals. In general, the low-temperature processing is attractive for SnO₂ to broaden its applications for PSCs. However, it also increases the difficulty for obtaining the SnO₂ ETL with proper surface states and Sn/O ratio because of the complexity of chemical composition in precursor and surface chemistry. These complexities associated with the chemical composition, structure and surface chemistry make it difficult to reliably secure the best fabrication conditions for certain purposes. It is worth noting that preparing the crystallographically perfect SnO₂—such as minimizing defects and obtaining stoichiometric SnO₂—is likely not enough for producing the optimum SnO₂ ETL for PSCs, because the surface energy level, band alignment, and electrical and optical properties may not be ideal for PSCs. Thus, identifying suitable deposition methods and advanced strategies for SnO₂ ETL fabrication is essential. We expect that the key to form a high-quality SnO₂ film can benefit from previous advances on solution processing by controlling both the nucleation process to form a compact dense film, and the reaction/growth pathway from intermediate species to the final SnO₂ film. Furthermore, the incomplete and reactive surface of SnO₂ can cause unexpected reactions at the SnO₂/perovskite interface, and such reactions can affect photovoltaic performance and stability of PSCs. With recent advances on SnO₂ ETL development for PSCs, engineering the SnO₂/perovskite interface has clearly become a critical factor for making efficient and stable n-i-p PSCs.

Several recent breakthroughs have pointed out promising approaches along these research directions to improve SnO₂ and SnO₂/perovskite interfacial properties.^[23, 31, 114, 144] Examples include using a polymer binder with colloidal SnO₂ deposition to form a dense and conformal SnO₂ ETL on textured FTO with minimized optical loss,^[144] modulating the formation of various Sn intermediate species by adjusting the pH of the reaction solution to control the defect states of the CBD SnO₂ ETL,^[23] and interfacial engineering based on a coherent FASnCl_x interlayer and SAM layer to make better interactions between SnO₂ and perovskite.^[31, 114] From those recent breakthrough studies, we can establish a checklist for further development of SnO₂: 1) minimizing the optical losses with a contiguous and conformal deposition on a textured substrate; 2) tuning the optimum Sn/O ratio in SnO_{2-x} (0<x<2), which strongly correlates to the physical/chemical/electronic properties of SnO₂; 3) reducing the unexpected reactions between SnO₂ and perovskite; and 4) developing strategies to enhance beneficial interactions between SnO₂ and perovskite for an improved interface. Overall, an ideal SnO₂ ETL is expected to be deposited along the textured FTO substrate as a dense and conformal film with a proper SnO₂/perovskite interlayer or interface region.

This article is protected by copyright. All rights reserved.

It is worth noting that despite extensive efforts over the past decade, it remains challenging to establish universal methods for controlling and engineering the surface of SnO₂ ETL. It is important to find out how each species exist on the SnO₂ surface react with perovskite to pinpoint the removal targets causing the problem at the SnO₂/perovskite interface. To evaluate these delicate and complex surface characteristics, both experimental and theoretical surface studies should be combined to provide guidance to enable the desired surface features of SnO₂ and to understand the reactions at SnO₂/perovskite interface.

9. Conclusion

In summary, the advances on the development of SnO₂ ETLs in recent years have repeatedly pushed forward the record PCE for single-junction PSCs, reaching close to 26%. Preparation methods and various passivation strategies are critical to ensuring the structural and electronic properties of SnO₂ ETLs are suitable for n-i-p PSCs. Overall, SnO₂ has several attractive features as an effective ETL, including good conductivity, high transparency, suitable band energy levels, and low-temperature processing; these factors have collectively enabled wide adoption of SnO₂ for the development of efficient n-i-p PSCs. With the maturing of various SnO₂ deposition techniques, it has become increasingly important for the development in surface treatment and surface passivation strategies to further enhance the device performance towards single-junction limit for PSCs. Furthermore, various SnO₂ deposition and treatment techniques have been also expanded and developed for different device architectures, including scalable and flexible devices.

Acknowledgements

The work was supported by the U.S. Department of Energy under Contract no. DE-AC36-08GO28308 with Alliance for Sustainable Energy, Limited Liability Company (LLC), the Manager and Operator of the National Renewable Energy Laboratory. The authors acknowledge the support from DE-FOA-0002064 and Award Number DE-EE0008790, funded by the U.S. Department of Energy, Office of Energy Efficiency and Renewable Energy, Solar Energy Technologies Office. The views expressed in the article do not necessarily represent the views of the DOE or the U.S. Government.

Received: ((will be filled in by the editorial staff))

Revised: ((will be filled in by the editorial staff))

Published online: ((will be filled in by the editorial staff))

Accepted Article

This article is protected by copyright. All rights reserved.

ReferencesUncategorized References

- [1] M. Liu, M. B. Johnston, H. J. Snaith, *Nature* 2013, 501, 395.
- [2] J. Y. Kim, J. W. Lee, H. S. Jung, H. Shin, N. G. Park, *Chem Rev* 2020, 120, 7867.
- [3] H. S. Kim, C. R. Lee, J. H. Im, K. B. Lee, T. Moehl, A. Marchioro, S. J. Moon, R. Humphry-Baker, J. H. Yum, J. E. Moser, M. Grätzel, N. G. Park, *Sci Rep* 2012, 2, 591.
- [4] M. A. Green, E. D. Dunlop, J. Hohl-Ebinger, M. Yoshita, N. Kopidakis, X. Hao, *Progress in Photovoltaics: Research and Applications* 2020, 28, 629.
- [5] M. M. Lee, J. Teuscher, T. Miyasaka, T. N. Murakami, H. J. Snaith, *Science* 2012, 338, 643.
- [6] E. H. Anaraki, A. Kermanpur, L. Steier, K. Domanski, T. Matsui, W. Tress, M. Saliba, A. Abate, M. Grätzel, A. Hagfeldt, J.-P. Correa-Baena, *Energy & Environmental Science* 2016, 9, 3128.
- [7] A. Kojima, K. Teshima, Y. Shirai, T. Miyasaka, *Journal of the American Chemical Society* 2009, 131, 6050.
- [8] S. Yun, Y. Qin, A. R. Uhl, N. Vlachopoulos, M. Yin, D. Li, X. Han, A. Hagfeldt, *Energy & Environmental Science* 2018, 11, 476.
- [9] U. Bach, D. Lupo, P. Comte, J. E. Moser, F. Weissörtel, J. Salbeck, H. Spreitzer, M. Grätzel, *Nature* 1998, 395, 583.
- [10] M. Grätzel, *MRS Bulletin* 2005, 30, 23.
- [11] V. E. Madhavan, I. Zimmermann, C. Roldán-Carmona, G. Grancini, M. Buffiere, A. Belaidi, M. K. Nazeeruddin, *ACS Energy Letters* 2016, 1, 1112.
- [12] C. W. Myung, G. Lee, K. S. Kim, *Journal of Materials Chemistry A* 2018, 6, 23071.
- [13] M. Zhu, W. Liu, W. Ke, L. Xie, P. Dong, F. Hao, *ACS Appl Mater Interfaces* 2019, 11, 666.
- [14] H. Yoon, S. M. Kang, J.-K. Lee, M. Choi, *Energy & Environmental Science* 2016, 9, 2262.
- [15] W. Ke, G. Fang, Q. Liu, L. Xiong, P. Qin, H. Tao, J. Wang, H. Lei, B. Li, J. Wan, G. Yang, Y. Yan, *J Am Chem Soc* 2015, 137, 6730.
- [16] J. Dou, Y. Zhang, Q. Wang, A. Abate, Y. Li, M. Wei, *Chem Commun (Camb)* 2019, 55, 14673.
- [17] Q. Dong, Y. Shi, K. Wang, Y. Li, S. Wang, H. Zhang, Y. Xing, Y. Du, X. Bai, T. Ma, *The Journal of Physical Chemistry C* 2015, 119, 10212.
- [18] J. Han, H. Kwon, E. Kim, D.-W. Kim, H. J. Son, D. H. Kim, *Journal of Materials Chemistry A* 2020, 8, 2105.
- [19] Q. Jiang, X. Zhang, J. You, *Small* 2018, 14, 1801154.

This article is protected by copyright. All rights reserved.

- [20] C. Altinkaya, E. Aydin, E. Ugur, F. H. Isikgor, A. S. Subbiah, M. De Bastiani, J. Liu, A. Babayigit, T. G. Allen, F. Laquai, A. Yildiz, S. De Wolf, *Advanced Materials* 2021, 33, 2005504.
- [21] Y. Chen, Q. Meng, L. Zhang, C. Han, H. Gao, Y. Zhang, H. Yan, *Journal of Energy Chemistry* 2019, 35, 144.
- [22] P. Wu, S. Wang, X. Li, F. Zhang, *Journal of Materials Chemistry A* 2021, 9, 19554.
- [23] J. J. Yoo, G. Seo, M. R. Chua, T. G. Park, Y. Lu, F. Rotermund, Y. K. Kim, C. S. Moon, N. J. Jeon, J. P. Correa-Baena, V. Bulovic, S. S. Shin, M. G. Bawendi, J. Seo, *Nature* 2021, 590, 587.
- [24] G. Yang, C. Chen, F. Yao, Z. Chen, Q. Zhang, X. Zheng, J. Ma, H. Lei, P. Qin, L. Xiong, W. Ke, G. Li, Y. Yan, G. Fang, *Adv Mater* 2018, 30, e1706023.
- [25] P. Zhu, S. Gu, X. Luo, Y. Gao, S. Li, J. Zhu, H. Tan, *Advanced Energy Materials* 2019, 10.
- [26] W. Ke, D. Zhao, A. J. Cimaroli, C. R. Grice, P. Qin, Q. Liu, L. Xiong, Y. Yan, G. Fang, *Journal of Materials Chemistry A* 2015, 3, 24163.
- [27] Q. Jiang, Z. Chu, P. Wang, X. Yang, H. Liu, Y. Wang, Z. Yin, J. Wu, X. Zhang, J. You, *Adv Mater* 2017, 29.
- [28] D. Yang, R. Yang, K. Wang, C. Wu, X. Zhu, J. Feng, X. Ren, G. Fang, S. Priya, S. F. Liu, *Nat Commun* 2018, 9, 3239.
- [29] K. Ma, H. R. Atapattu, Q. Zhao, Y. Gao, B. P. Finkenauer, K. Wang, K. Chen, S. M. Park, A. H. Coffey, C. Zhu, L. Huang, K. R. Graham, J. Mei, L. Dou, *Adv Mater* 2021, 33, e2100791.
- [30] J. P. Correa Baena, L. Steier, W. Tress, M. Saliba, S. Neutzner, T. Matsui, F. Giordano, T. J. Jacobsson, A. R. Srimath Kandada, S. M. Zakeeruddin, A. Petrozza, A. Abate, M. K. Nazeeruddin, M. Grätzel, A. Hagfeldt, *Energy & Environmental Science* 2015, 8, 2928.
- [31] H. Min, D. Y. Lee, J. Kim, G. Kim, K. S. Lee, J. Kim, M. J. Paik, Y. K. Kim, K. S. Kim, M. G. Kim, T. J. Shin, S. Il Seok, *Nature* 2021, 598, 444.
- [32] J. A. Christians, P. Schulz, J. S. Tinkham, T. H. Schloemer, S. P. Harvey, B. J. Tremolet de Villers, A. Sellinger, J. J. Berry, J. M. Luther, *Nature Energy* 2018, 3, 68.
- [33] S. Thampy, B. Zhang, K.-H. Hong, K. Cho, J. W. P. Hsu, *ACS Energy Letters* 2020, 5, 1147.
- [34] E. Aydin, M. De Bastiani, S. De Wolf, *Adv Mater* 2019, 31, e1900428.
- [35] G. Tong, L. K. Ono, Y. Liu, H. Zhang, T. Bu, Y. Qi, *Nanomicro Lett* 2021, 13, 155.
- [36] Q. Jiang, Y. Zhao, X. Zhang, X. Yang, Y. Chen, Z. Chu, Q. Ye, X. Li, Z. Yin, J. You, *Nature Photonics* 2019, 13, 460.
- [37] Y.-W. Jang, S. Lee, K. M. Yeom, K. Jeong, K. Choi, M. Choi, J. H. Noh, *Nature Energy* 2021, 6, 63.

This article is protected by copyright. All rights reserved.

- [38] Z. Liu, L. Qiu, L. K. Ono, S. He, Z. Hu, M. Jiang, G. Tong, Z. Wu, Y. Jiang, D.-Y. Son, Y. Dang, S. Kazaoui, Y. Qi, *Nature Energy* 2020, 5, 596.
- [39] X. Liu, K.-W. Tsai, Z. Zhu, Y. Sun, C.-C. Chueh, A. K. Y. Jen, *Advanced Materials Interfaces* 2016, 3.
- [40] K.-H. Jung, J.-Y. Seo, S. Lee, H. Shin, N.-G. Park, *Journal of Materials Chemistry A* 2017, 5, 24790.
- [41] Y. Bai, D. Xing, H. Luo, Q.-S. Jiang, L. Yuan, X. Ge, X. Yang, Y. Zhang, F. Xie, K. Yan, *Applied Surface Science* 2021, 552.
- [42] L. Zuo, H. Guo, D. W. deQuilettes, S. Jariwala, N. D. Marco, S. Dong, R. DeBlock, D. S. Ginger, B. Dunn, M. Wang, Y. Yang, *Science Advances* 2017, 3, e1700106.
- [43] J. Song, E. Zheng, J. Bian, X.-F. Wang, W. Tian, Y. Sanehira, T. Miyasaka, *Journal of Materials Chemistry A* 2015, 3, 10837.
- [44] Q. Jiang, L. Zhang, H. Wang, X. Yang, J. Meng, H. Liu, Z. Yin, J. Wu, X. Zhang, J. You, *Nature Energy* 2016, 2.
- [45] Z. Xiong, X. Chen, B. Zhang, G. O. Odunmbaku, Z. Ou, B. Guo, K. Yang, Z. Kan, S. Lu, S. Chen, N. A. N. Ouedraogo, Y. Cho, C. Yang, J. Chen, K. Sun, *Advanced Materials* 2021, n/a, 2106118.
- [46] Y. Kuang, V. Zardetto, R. van Gils, S. Karwal, D. Koushik, M. A. Verheijen, L. E. Black, C. Weijtens, S. Veenstra, R. Andriessen, W. M. M. Kessels, M. Creatore, *ACS Appl Mater Interfaces* 2018, 10, 30367.
- [47] J.-P. Correa-Baena, W. Tress, K. Domanski, E. H. Anaraki, S.-H. Turren-Cruz, B. Roose, P. P. Boix, M. Grätzel, M. Saliba, A. Abate, A. Hagfeldt, *Energy & Environmental Science* 2017, 10, 1207.
- [48] Z. M. Jarzebski, J. P. Marton, *Journal of The Electrochemical Society* 1976, 123, 199C.
- [49] L. Gracia, A. Beltrán, J. Andrés, *The Journal of Physical Chemistry B* 2007, 111, 6479.
- [50] S. Das, V. Jayaraman, *Progress in Materials Science* 2014, 66, 112.
- [51] C. Kilic, A. Zunger, *Phys Rev Lett* 2002, 88, 095501.
- [52] A. M. Ganose, D. O. Scanlon, *Journal of Materials Chemistry C* 2016, 4, 1467.
- [53] H. P. Boehm, *Discussions of the Faraday Society* 1971, 52, 264.
- [54] Y. Yuan, Y. Wang, M. Wang, J. Liu, C. Pei, B. Liu, H. Zhao, S. Liu, H. Yang, *Sci Rep* 2017, 7, 1231.
- [55] M. Stolterfoht, P. Caprioglio, C. M. Wolff, J. A. Márquez, J. Nordmann, S. Zhang, D. Rothhardt, U. Hörmann, Y. Amir, A. Redinger, L. Kegelmann, F. Zu, S. Albrecht, N. Koch, T. Kirchartz, M. Saliba, T. Unold, D. Neher, *Energy & Environmental Science* 2019, 12, 2778.

This article is protected by copyright. All rights reserved.

- [56] S. Y. Park, M. Y. Baek, Y. Ju, D. H. Kim, C. S. Moon, J. H. Noh, H. S. Jung, *J Phys Chem Lett* 2018, 9, 5460.
- [57] Y. Sun, Z. Pang, Y. Quan, D. Han, X. Zhang, X. Ge, F. Wang, Y. Sun, J. Yang, L. Yang, *Chemical Engineering Journal* 2021, 413.
- [58] J. Barbe, M. L. Tietze, M. Neophytou, B. Murali, E. Alarousu, A. E. Labban, M. Abulikemu, W. Yue, O. F. Mohammed, I. McCulloch, A. Amassian, S. Del Gobbo, *ACS Appl Mater Interfaces* 2017, 9, 11828.
- [59] W. Zhou, Y. Liu, Y. Yang, P. Wu, *The Journal of Physical Chemistry C* 2014, 118, 6448.
- [60] U. Wurfel, A. Cuevas, P. Wurfel, *IEEE Journal of Photovoltaics* 2015, 5, 461.
- [61] J. K. Katahara, H. W. Hillhouse, *Journal of Applied Physics* 2014, 116.
- [62] H. J. Snaith, A. Abate, J. M. Ball, G. E. Eperon, T. Leijtens, N. K. Noel, S. D. Stranks, J. T. Wang, K. Wojciechowski, W. Zhang, *J Phys Chem Lett* 2014, 5, 1511.
- [63] M. De Bastiani, E. Aydin, T. Allen, D. Walter, A. Fell, J. Peng, N. Gasparini, J. Troughton, D. Baran, K. Weber, T. P. White, S. De Wolf, *Advanced Electronic Materials* 2019, 5.
- [64] L. Kavan, L. Steier, M. Grätzel, *The Journal of Physical Chemistry C* 2016, 121, 342.
- [65] J. H. Won, S. H. Han, B. K. Park, T.-M. Chung, J. H. Han, *Coatings* 2020, 10.
- [66] C. Wang, D. Zhao, C. R. Grice, W. Liao, Y. Yu, A. Cimaroli, N. Shrestha, P. J. Roland, J. Chen, Z. Yu, P. Liu, N. Cheng, R. J. Ellingson, X. Zhao, Y. Yan, *Journal of Materials Chemistry A* 2016, 4, 12080.
- [67] Q. Dong, Y. Shi, C. Zhang, Y. Wu, L. Wang, *Nano Energy* 2017, 40, 336.
- [68] V. Rohnacher, F. Ullrich, H. Eggers, F. Schackmar, S. Hell, A. Salazar, C. Huck, G. Hernandez-Sosa, U. W. Paetzold, W. Jaegermann, A. Pucci, *Advanced Materials Technologies* 2020, 6.
- [69] A. S. Subbiah, N. Mathews, S. Mhaisalkar, S. K. Sarkar, *ACS Energy Letters* 2018, 3, 1482.
- [70] L. Huang, X. Sun, C. Li, J. Xu, R. Xu, Y. Du, J. Ni, H. Cai, J. Li, Z. Hu, J. Zhang, *ACS Applied Materials & Interfaces* 2017, 9, 21909.
- [71] B. Taheri, F. De Rossi, G. Lucarelli, L. A. Castriotta, A. Di Carlo, T. M. Brown, F. Brunetti, *ACS Appl Energy Mater* 2021, 4, 4507.
- [72] T. Bu, J. Li, F. Zheng, W. Chen, X. Wen, Z. Ku, Y. Peng, J. Zhong, Y. B. Cheng, F. Huang, *Nat Commun* 2018, 9, 4609.
- [73] J. Zhang, C. Bai, Y. Dong, W. Shen, Q. Zhang, F. Huang, Y.-B. Cheng, J. Zhong, *Chemical Engineering Journal* 2021, 425.
- [74] L. Mai, D. Zanders, E. Subasi, E. Ciftiyurek, C. Hoppe, D. Rogalla, W. Gilbert, T. L. Arcos, K. Schierbaum, G. Grundmeier, C. Bock, A. Devi, *ACS Appl Mater Interfaces* 2019, 11, 3169.

This article is protected by copyright. All rights reserved.

- [75] Z. Song, W. Bi, X. Zhuang, Y. Wu, B. Zhang, X. Chen, C. Chen, Q. Dai, H. Song, *Solar RRL* 2019, 4.
- [76] Y. Guo, X. Yin, J. Liu, W. Chen, S. Wen, M. Que, H. Xie, Y. Yang, W. Que, B. Gao, *Organic Electronics* 2019, 65, 207.
- [77] Y. Porte, R. Maller, H. Faber, H. N. AlShareef, T. D. Anthopoulos, M. A. McLachlan, *Journal of Materials Chemistry C* 2016, 4, 758.
- [78] C. Altinkaya, E. Aydin, E. Ugur, F. H. Isikgor, A. S. Subbiah, M. De Bastiani, J. Liu, A. Babayigit, T. G. Allen, F. Laquai, A. Yildiz, S. De Wolf, *Adv Mater* 2021, 33, e2005504.
- [79] D. Han, B. Jiang, J. Feng, Y. Yin, W. Wang, *Angewandte Chemie International Edition* 2017, 56, 7792.
- [80] J. Chen, N. G. Park, *Adv Mater* 2019, 31, e1803019.
- [81] K. Liu, S. Chen, J. Wu, H. Zhang, M. Qin, X. Lu, Y. Tu, Q. Meng, X. Zhan, *Energy & Environmental Science* 2018, 11, 3463.
- [82] Z. Qian, L. Chen, J. Wang, L. Wang, Y. Xia, X. Ran, P. Li, Q. Zhong, L. Song, P. Müller-Buschbaum, Y. Chen, H. Zhang, *Advanced Materials Interfaces* 2021, 8.
- [83] H. Wang, C. Zhu, L. Liu, S. Ma, P. Liu, J. Wu, C. Shi, Q. Du, Y. Hao, S. Xiang, H. Chen, P. Chen, Y. Bai, H. Zhou, Y. Li, Q. Chen, *Adv Mater* 2019, 31, e1904408.
- [84] M. Zhang, F. Wu, D. Chi, K. Shi, S. Huang, *Materials Advances* 2020, 1, 617.
- [85] S. Shao, M. A. Loi, *Advanced Materials Interfaces* 2019, 7.
- [86] P. Zhao, Z. Lin, J. Wang, M. Yue, J. Su, J. Zhang, J. Chang, Y. Hao, *ACS Applied Energy Materials* 2019, 2, 4504.
- [87] C. Ding, Y. Zhang, F. Liu, Y. Kitabatake, S. Hayase, T. Toyoda, K. Yoshino, T. Minemoto, K. Katayama, Q. Shen, *Nano Energy* 2018, 53, 17.
- [88] Y. Raoui, H. Ez-Zahraouy, S. Kazim, S. Ahmad, *Journal of Energy Chemistry* 2021, 54, 822.
- [89] P. Hang, J. Xie, G. Li, Y. Wang, D. Fang, Y. Yao, D. Xie, C. Cui, K. Yan, J. Xu, D. Yang, X. Yu, *iScience* 2019, 21, 217.
- [90] S. Thampy, W. Xu, J. W. P. Hsu, *J Phys Chem Lett* 2021, 12, 8495.
- [91] G. Mathiazhagan, A. Seeber, T. Gengenbach, S. Mastroianni, D. Vak, A. S. R. Chesman, M. Gao, D. Angmo, A. Hinsch, *Solar RRL* 2020, 4.
- [92] B. Roose, J.-P. C. Baena, K. C. Gödel, M. Graetzel, A. Hagfeldt, U. Steiner, A. Abate, *Nano Energy* 2016, 30, 517.

This article is protected by copyright. All rights reserved.

- [93] W. Li, W. Zhang, S. Van Reenen, R. J. Sutton, J. Fan, A. A. Haghighirad, M. B. Johnston, L. Wang, H. J. Snaith, *Energy & Environmental Science* 2016, 9, 490.
- [94] C. Zhu, X. Niu, Y. Fu, N. Li, C. Hu, Y. Chen, X. He, G. Na, P. Liu, H. Zai, Y. Ge, Y. Lu, X. Ke, Y. Bai, S. Yang, P. Chen, Y. Li, M. Sui, L. Zhang, H. Zhou, Q. Chen, *Nat Commun* 2019, 10, 815.
- [95] N. Rolston, A. D. Printz, J. M. Tracy, H. C. Weerasinghe, D. Vak, L. J. Haur, A. Priyadarshi, N. Mathews, D. J. Slotcavage, M. D. McGehee, R. E. Kalan, K. Zielinski, R. L. Grimm, H. Tsai, W. Nie, A. D. Mohite, S. Gholipour, M. Saliba, M. Grätzel, R. H. Dauskardt, *Advanced Energy Materials* 2017, 8.
- [96] W. Yang, D. Zhong, M. Shi, S. Qu, H. Chen, *iScience* 2019, 22, 534.
- [97] J. Wu, Y. Cui, B. Yu, K. Liu, Y. Li, H. Li, J. Shi, H. Wu, Y. Luo, D. Li, Q. Meng, *Advanced Functional Materials* 2019, 29.
- [98] G. Xie, X. Lu, J. Duan, Y. Dong, X. Jiang, F. Tu, Y. Duan, Q. Tang, *Journal of Materials Chemistry A* 2021, 9, 15003.
- [99] Y. Huang, S. Li, C. Wu, S. Wang, C. Wang, R. Ma, *Chemical Physics Letters* 2020, 745.
- [100] M. Park, J.-Y. Kim, H. J. Son, C.-H. Lee, S. S. Jang, M. J. Ko, *Nano Energy* 2016, 26, 208.
- [101] A. Ponzoni, *Sensors (Basel)* 2020, 21.
- [102] W. Gong, H. Guo, H. Zhang, J. Yang, H. Chen, L. Wang, F. Hao, X. Niu, *Journal of Materials Chemistry C* 2020, 8, 11638.
- [103] S. Zhang, H. Gu, S.-C. Chen, Q. Zheng, *Journal of Materials Chemistry C* 2021, 9, 4240.
- [104] Z. Li, L. Wang, R. Liu, Y. Fan, H. Meng, Z. Shao, G. Cui, S. Pang, *Advanced Energy Materials* 2019, 9.
- [105] J. Zhuang, P. Mao, Y. Luan, N. Chen, X. Cao, G. Niu, F. Jia, F. Wang, S. Cao, J. Wang, *Advanced Functional Materials* 2021, 31.
- [106] X. Liu, Y. Zhang, L. Shi, Z. Liu, J. Huang, J. S. Yun, Y. Zeng, A. Pu, K. Sun, Z. Hameiri, J. A. Stride, J. Seidel, M. A. Green, X. Hao, *Advanced Energy Materials* 2018, 8.
- [107] K. Choi, J. Lee, H. I. Kim, C. W. Park, G.-W. Kim, H. Choi, S. Park, S. A. Park, T. Park, *Energy & Environmental Science* 2018, 11, 3238.
- [108] M. Hou, H. Zhang, Z. Wang, Y. Xia, Y. Chen, W. Huang, *ACS Appl Mater Interfaces* 2018, 10, 30607.
- [109] B. Tu, Y. Shao, W. Chen, Y. Wu, X. Li, Y. He, J. Li, F. Liu, Z. Zhang, Y. Lin, X. Lan, L. Xu, X. Shi, A. M. C. Ng, H. Li, L. W. Chung, A. B. Djurisic, Z. He, *Adv Mater* 2019, 31, e1805944.

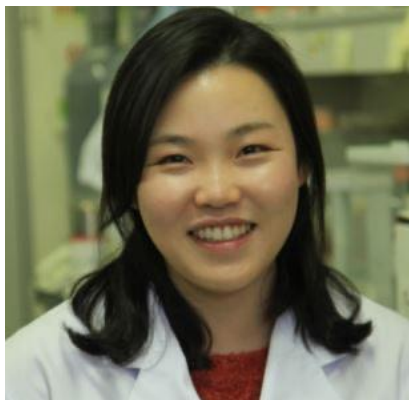
This article is protected by copyright. All rights reserved.

- [110] M. Abdi-Jalebi, Z. Andaji-Garmaroudi, S. Cacovich, C. Stavrakas, B. Philippe, J. M. Richter, M. Alsari, E. P. Booker, E. M. Hutter, A. J. Pearson, S. Lilliu, T. J. Savenije, H. Rensmo, G. Divitini, C. Ducati, R. H. Friend, S. D. Stranks, *Nature* 2018, 555, 497.
- [111] Z. Liu, K. Deng, J. Hu, L. Li, *Angew Chem Int Ed Engl* 2019, 58, 11497.
- [112] E. H. Jung, B. Chen, K. Bertens, M. Vafaie, S. Teale, A. Proppe, Y. Hou, T. Zhu, C. Zheng, E. H. Sargent, *ACS Energy Letters* 2020, 5, 2796.
- [113] L. Zuo, Q. Chen, N. De Marco, Y. T. Hsieh, H. Chen, P. Sun, S. Y. Chang, H. Zhao, S. Dong, Y. Yang, *Nano Lett* 2017, 17, 269.
- [114] Z. Dai, S. K. Yadavalli, M. Chen, A. Abbaspourtamijani, Y. Qi, N. P. Padture, *Science* 2021, 372, 618.
- [115] Y. Shi, H. Zhang, X. Tong, X. Hou, F. Li, Y. Du, S. Wang, Q. Zhang, P. Liu, X. Zhao, *Solar RRL* 2021, 5.
- [116] G. Yang, C. Wang, H. Lei, X. Zheng, P. Qin, L. Xiong, X. Zhao, Y. Yan, G. Fang, *Journal of Materials Chemistry A* 2017, 5, 1658.
- [117] W. Hui, Y. Yang, Q. Xu, H. Gu, S. Feng, Z. Su, M. Zhang, J. Wang, X. Li, J. Fang, F. Xia, Y. Xia, Y. Chen, X. Gao, W. Huang, *Adv Mater* 2020, 32, e1906374.
- [118] M. Hu, L. Zhang, S. She, J. Wu, X. Zhou, X. Li, D. Wang, J. Miao, G. Mi, H. Chen, Y. Tian, B. Xu, C. Cheng, *Solar RRL* 2020, 4, 1900331.
- [119] Y. Chen, C. Xu, J. Xiong, Z. Zhang, X. Zhang, J. Yang, X. Xue, D. Yang, J. Zhang, *Organic Electronics* 2018, 58, 294.
- [120] J. Dagar, S. Castro-Hermosa, G. Lucarelli, F. Cacialli, T. M. Brown, *Nano Energy* 2018, 49, 290.
- [121] R. A. Awni, Z. Song, C. Chen, C. Li, C. Wang, M. A. Razooqi, L. Chen, X. Wang, R. J. Ellingson, J. V. Li, Y. Yan, *Joule* 2020, 4, 644.
- [122] J. Wang, K. Datta, C. H. L. Weijtens, M. M. Wienk, R. A. J. Janssen, *Advanced Functional Materials* 2019, 29.
- [123] J. Ma, G. Yang, M. Qin, X. Zheng, H. Lei, C. Chen, Z. Chen, Y. Guo, H. Han, X. Zhao, G. Fang, *Adv Sci (Weinh)* 2017, 4, 1700031.
- [124] M. Abuhelaiqa, N. Shibayama, X.-X. Gao, H. Kanda, M. K. Nazeeruddin, *ACS Applied Energy Materials* 2021, 4, 3424.
- [125] U. Khan, T. Iqbal, M. Khan, R. Wu, *Solar Energy* 2021, 223, 346.
- [126] S. S. Mali, J. V. Patil, H. Arandiyani, C. K. Hong, *Journal of Materials Chemistry A* 2019, 7, 17516.

This article is protected by copyright. All rights reserved.

- [127] N. Arora, M. I. Dar, S. Akin, R. Uchida, T. Baumeler, Y. Liu, S. M. Zakeeruddin, M. Grätzel, *Small* 2019, 15, e1904746.
- [128] Z. Wang, X. Zhu, J. Feng, C. Wang, C. Zhang, X. Ren, S. Priya, S. Liu, D. Yang, *Advanced Science* 2021, 8, 2002860.
- [129] Y. Dkhissi, S. Meyer, D. Chen, H. C. Weerasinghe, L. Spiccia, Y. B. Cheng, R. A. Caruso, *ChemSusChem* 2016, 9, 687.
- [130] Z. Li, L. Wang, R. Liu, Y. Fan, H. Meng, Z. Shao, G. Cui, S. Pang, *Advanced Energy Materials* 2019, 9, 1902142.
- [131] H. Baig, H. Kanda, A. M. Asiri, M. K. Nazeeruddin, T. Mallick, *Sustainable Energy & Fuels* 2020, 4, 528.
- [132] D.-K. Lee, D.-N. Jeong, T. K. Ahn, N.-G. Park, *ACS Energy Letters* 2019, 4, 2393.
- [133] L. Chao, T. Niu, W. Gao, C. Ran, L. Song, Y. Chen, W. Huang, *Adv Mater* 2021, 33, e2005410.
- [134] B. Taheri, E. Calabrò, F. Matteocci, D. Di Girolamo, G. Cardone, A. Liscio, A. Di Carlo, F. Brunetti, *Energy Technology* 2020, 8.
- [135] J. B. Whitaker, D. H. Kim, Bryon W. Larson, F. Zhang, J. J. Berry, M. F. A. M. van Hest, K. Zhu, *Sustainable Energy & Fuels* 2018, 2, 2442.
- [136] Y. Hu, S. Si, A. Mei, Y. Rong, H. Liu, X. Li, H. Han, *Solar RRL* 2017, 1.
- [137] G. S. Han, J. Kim, S. Bae, S. Han, Y. J. Kim, O. Y. Gong, P. Lee, M. J. Ko, H. S. Jung, *ACS Energy Letters* 2019, 4, 1845.
- [138] T. Bu, X. Liu, J. Li, W. Huang, Z. Wu, F. Huang, Y.-B. Cheng, J. Zhong, *Solar RRL* 2019, 4.
- [139] H. S. Jung, G. S. Han, N.-G. Park, M. J. Ko, *Joule* 2019, 3, 1850.
- [140] M. Epifani, J. Arbiol, T. Andreu, J. R. Morante, *European Journal of Inorganic Chemistry* 2008, 2008, 859.
- [141] H. Xie, X. Yin, P. Chen, J. Liu, C. Yang, W. Que, G. Wang, *Materials Letters* 2019, 234, 311.
- [142] C. Wang, L. Guan, D. Zhao, Y. Yu, C. R. Grice, Z. Song, R. A. Awni, J. Chen, J. Wang, X. Zhao, Y. Yan, *ACS Energy Letters* 2017, 2, 2118.
- [143] Q. Dong, C. Zhu, M. Chen, C. Jiang, J. Guo, Y. Feng, Z. Dai, S. K. Yadavalli, M. Hu, X. Cao, Y. Li, Y. Huang, Z. Liu, Y. Shi, L. Wang, N. P. Padture, Y. Zhou, *Nat Commun* 2021, 12, 973.
- [144] M. Kim, J. Jeong, H. Lu, K. Lee Tae, T. Eickemeyer Felix, Y. Liu, W. Choi In, J. Choi Seung, Y. Jo, H.-B. Kim, S.-I. Mo, Y.-K. Kim, H. Lee, G. An Na, S. Cho, R. Tress Wolfgang, M. Zakeeruddin Shaik, A. Hagfeldt, Y. Kim Jin, M. Grätzel, S. Kim Dong, *Science* 2022, 375, 302.

This article is protected by copyright. All rights reserved.



So Yeon Park is currently a postdoctoral researcher in the Chemistry and Nanoscience Center at National Renewable Energy Laboratory. She received a Ph.D. in advanced materials science and engineering from Sungkyunkwan University in 2019. She is broadly interested in synthesis of low-dimensional inorganic materials, and optoelectronic materials and the surface engineering of those materials for various applications. Her current research interests mainly concentrate on the fabrication of highly efficient and stable perovskite solar cells, and the development of sustainable and closed process loop for perovskite solar cells.



Kai Zhu is a senior scientist in the Chemistry and Nanoscience Science Center at the National Renewable Energy Laboratory (NREL). He received his PhD degree in physics from Syracuse University in 2003. His research interests have included characterization and modeling of hydrogenated amorphous silicon thin film solar cell, III-V wide-bandgap light emitting diodes, dye-sensitized solar cells, and Li-ion batteries and supercapacitors. His current research focuses on perovskite solar cells, including material development, device fabrication, and fundamental characterization on charge-carrier dynamics and device operating principles.

This article is protected by copyright. All rights reserved.

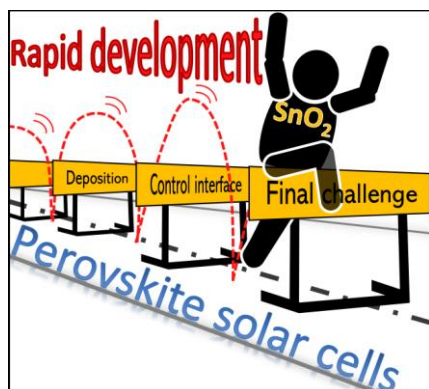
TOC Graphic

This review summarizes the recent advances of SnO₂-based perovskite solar cells (PSCs) and the related interface optimization strategies and applications. We discuss the fundamental properties of SnO₂ with a focus on the defect chemistry, and various preparation methods for improving SnO₂ and SnO₂/perovskite interface. Finally, the challenges and opportunities for further development of SnO₂-based PSCs are provided.

Keyword: Additives; Perovskite Solar Cells; Electron Transport Layer; Semiconducting Oxide Layer; SnO₂

So Yeon Park, Kai Zhu*

Advances in SnO₂ for Efficient and Stable n-i-p Perovskite Solar Cells



This article is protected by copyright. All rights reserved.